Sippl, C., Schurr, B., Yuan, X., Mechie, J., Schneider, F. M., Gadoev, M., Orunbaev, S., Oimahmadov, I., Haberland, C., Abdybachaev, U., Minaev, V., Negmatullaev, S., Radjabov, N. (2013): Geometry of the Pamir-Hindu Kush intermediate-depth earthquake zone from local seismic data. - Journal of Geophysical Research, 118, 4, 1438-1457

DOI: 10.1002/jgrb.50128

JOURNAL OF GEOPHYSICAL RESEARCH: SOLID EARTH, VOL. 118, 1438–1457, doi:10.1002/jgrb.50128, 2013

Geometry of the Pamir-Hindu Kush intermediate-depth earthquake zone from local seismic data

C. Sippl,[1] B. Schurr,[1] X. Yuan,[1] J. Mechie,[1] F. M. Schneider,[1] M. Gadoev,[2] S. Orunbaev,[3] I. Oimahmadov,[2] C. Haberland,[1] U. Abdybachaev,[3] V. Minaev,[2] S. Negmatullaev,[4] and N. Radjabov[2]

Received 5 October 2012; revised 8 February 2013; accepted 11 February 2013; published 8 April 2013.

[1] We present new seismicity images based on a two-year seismic deployment in the Pamir and SW Tien Shan. A total of 9532 earthquakes were detected, located, and rigorously assessed in a multistage automatic procedure utilizing state-of-the-art picking algorithms, waveform cross-correlation, and multi-event relocation. The obtained catalog provides new information on crustal seismicity and reveals the geometry and internal structure of the Pamir-Hindu Kush intermediate-depth seismic zone with improved detail and resolution. The relocated seismicity clearly defines at least two distinct planes: one beneath the Pamir and the other beneath the Hindu Kush, separated by a gap across which strike and dip directions change abruptly. The Pamir seismic zone forms a thin (approximately 10 km width), curviplanar arc that strikes east-west and dips south at its eastern end and then progressively turns by 90° to reach a north-south strike and a due eastward dip at its southwestern termination. Pamir deep seismicity outlines several streaks at depths between 70 and 240 km, with the deepest events occurring at its southwestern end. Intermediate-depth earthquakes are clearly separated from shallow crustal seismicity, which is confined to the uppermost 20–25 km. The Hindu Kush seismic zone extends from 40 to 250 km depth and generally strikes east-west, yet bends northeast, toward the Pamir, at its eastern end. It may be divided vertically into upper and lower parts separated by a gap at approximately 150 km depth. In the upper part, events form a plane that is 15–25 km thick in cross section and dips sub-vertically north to northwest. Seismic activity is more virile in the lower part, where several distinct clusters form a complex pattern of sub-parallel planes. The observed geometry could be reconciled either with a model of two-sided subduction of Eurasian and previously underthrusted Indian continental lithosphere or by a purely Eurasian origin of both Pamir and Hindu Kush seismic zones, which necessitates a contortion and oversteepening of the latter.

Citation: Sippl, C., et al. (2013), Geometry of the Pamir-Hindu Kush intermediate-depth earthquake zone from local seismic data, *J. Geophys. Res. Solid Earth*, *118*, 1438–1457, doi:10.1002/jgrb.50128.

1. Introduction

[2] Today's Himalaya-Tibet orogenic system is, to first order, the result of the ongoing indentation of a rigid cratonic block (India) into a mechanically weaker Eurasia [e.g., *Tapponnier et al*., 1982] following the closure of the Neo-Tethys ocean [*Patriat and Achache*, 1984; *Guillot*, 2003]. The tectonic evolution of the collision is complex and involves subduction/underthrusting of (greater) Indian lithosphere, possible slab break-off(s), distributed lithospheric shortening of both Eurasia and India as well as possible lithospheric delamination and continental-scale escape along large strike-slip systems [e.g., *Molnar and Tapponnier*, 1975; *Tapponnier and Molnar*, 1979; *Avouac and Tapponnier*, 1993; *Yin and Harrison*, 2000; *Chemenda et al*., 2000]. The lateral edges (syntaxes) of this Indian indenter have since created deformed regions of considerable complexity in their vicinity, which are less well understood than processes and structures along the indenter's front (Himalaya, Tibetan plateau). The ongoing convergence between India and Eurasia is currently to first order

Additional supporting information may be found in the online version of this article.

[1]Helmholtz Centre Potsdam—German Research Centre for Geosciences (GFZ), Potsdam, Germany.
[2]Geological Institute, Tajik Academy of Sciences, Dushanbe, Tajikistan.
[3]Central Asian Institute for Applied Geosciences (CAIAG), Bishkek, Kyrgyzstan.
[4]PMP International, Dushanbe, Tajikistan.

Corresponding author: C. Sippl, Helmholtz-Zentrum Potsdam, Deutsches GeoForschungsZentrum (GFZ) Am Telegrafenberg, 14473 Potsdam. (sippl@gfz-potsdam.de)

2169-9313/13/10.1002/jgrb.50128

accommodated by continental underthrusting of Indian lithosphere [*Nábelek et al.*, 2009; *Kind and Yuan*, 2010] and possibly lower crust [*Hetényi et al.*, 2007; *Wittlinger et al.*, 2009] beneath Eurasia and the internal shortening of Eurasia further north. However, there is some indication that parts of the Eurasian continent might likewise locally subduct or underthrust [e.g., *Burtman and Molnar*, 1993; *Kind et al*., 2002; *Wittlinger et al*., 2004; *Zhao et al*., 2011]. The Pamir-Hindu Kush region, which is situated north of the western Himalayan syntaxis, exhibits features that not only set it apart from the neighboring Himalaya-Tibet system but are globally unique and thereby raise some fundamental issues in our understanding of orogenic processes.

[3] The western Himalaya-Hindu Kush-Pamir system accommodated a similar amount of Cenozoic convergence as the Himalaya-Tibet system, albeit over a much shorter meridional width, resulting in a higher amount of upper plate shortening [*van Hinsbergen et al*., 2011, deduce 1050 km] as well as a probably higher amount of crust that vanished into the mantle. Lithospheric deformation is accompanied by vigorous intermediate-depth (up to nearly 300 km depth) earthquake activity [*Billington et al.*, 1977; *Pegler and Das*, 1998], which is, with the possible exception of Vrancea, Romania [*Ismail-Zadeh et al.*, 2012], globally unique within a continental collision zone far from any active oceanic subduction. Tibet, in comparison, is essentially aseismic at depths greater than 80 or 90 km (uppermost mantle). Intermediate-depth earthquakes in the Pamir-Hindu Kush stirred scientific curiosity since *Gutenberg and Richter* [1954] first reported their existence nearly six decades ago. Generally, these earthquakes are thought to attest to active mantle deformation at the edge of the India-Eurasia collision. The modes of deep lithospheric deformation during orogeny, however, are only poorly understood, and a great variety of processes have been shown to be theoretically possible in a number of studies based on numerical or analog modeling [e.g., *Toussaint et al*., 2004; *Burov and Yamato*, 2008; *Gray and Pysklywec*, 2012; *Chemenda et al*., 2000]. These include, in addition to the scenarios resembling classic oceanic subduction, lithospheric and/or lower crustal delamination [*Bird*, 1979] or convective downwelling of a drop-like lithospheric body into the mantle (Rayleigh-Taylor instability) [see *Houseman et al*., 1981]. However, comparison of these models to nature is difficult because of a lack of observations, not least because of the generally aseismic nature of orogenic mantle deformation, with the apparent exception of the Pamir-Hindu Kush. A variety of models attempting to explain the Pamir-Hindu Kush zone's peculiar geometry (along-strike overturning of dip) and dynamics have been proposed, but fundamental questions, e.g., whether it is related to subduction [e.g., *Billington et al*., 1977] or exists due to a mantle drip [*Koulakov*, 2011], whether continental [*Roecker*, 1982; *Burtman and Molnar*, 1993] or oceanic material [*Chatelain et al.*, 1980; *Pegler and Das*, 1998] hosts these earthquakes, or whether Pamir and Hindu Kush form one single [*Billington et al.*, 1977; *Pegler and Das*, 1998; *Pavlis and Das*, 2000] or two separate structures [*Chatelain et al.*, 1980; *Burtman and Molnar*, 1993; *Fan et al.*, 1994] outlined by seismic activity, have not been conclusively solved.

[4] Here we present a detailed seismicity distribution derived from the first modern, digital passive seismic data set collected in this remote region. In particular, we seek to clarify the exact geometry of the structures outlined by intermediate-depth seismicity in the Pamir and Hindu Kush by analyzing depth maps and cross-sections through the seismic zone. In interpreting the imaged structures and their implications, we attempt to provide a step toward the clarification of processes that have created this unique setting.

2. Tectonic Setting

[5] The Pamir-Hindu Kush region is situated directly north of the western syntaxis of the India-Eurasia collision system, marking the probable westernmost extent of the (Greater) Indian indenter penetrating into Eurasia. This collision, which initiated at 50–52 Ma [*Patriat and Achache*, 1984; *Guillot*, 2003; *van Hinsbergen et al.*, 2011] and has led to the creation of world's highest mountain ranges and largest plateaux, is presently ongoing with a convergence velocity of 34 mm/yr near the western syntaxis [*Molnar and Stock*, 2009; *DeMets et al.*, 2010]. The Pamir, a northward-convex mountain range, has presumably been moving north relative to the surrounding regions since about 25 Ma [*Sobel and Dumitru*, 1997], overriding the Tajik-Yarkand Basin [*Burtman and Molnar*, 1993], which previously connected the Tajik Depression in the west and the Tarim Basin in the east. It consists of roughly E-W trending structural belts that reflect a history of successive terrane accretion. These are commonly referred to as Northern (Paleozoic subduction-accretion complex), Central (Mesozoic platform rocks), and Southern (mostly Mesozoic metasediments) Pamir [*Burtman and Molnar*, 1993; *Schwab et al*., 2004; *Mechie et al*., 2012]. Correlation of the terranes and the sutures separating them from their counterparts in Tibet [e.g., *Yin and Harrison*, 2000] and Afghanistan [*Burtman and Molnar*, 1993] indicates a relative northward displacement of the entire Pamir by about 300 km. This northward displacement of the Pamir is accommodated by strike-slip faults along its flanks. In the west, these are the Chaman Fault [*Tapponnier et al.*, 1981]; in the further north, the Darvaz Fault [*Burtman and Molnar*, 1993; *Trifonov*, 1978]; and in the east, the Karakorum Fault [e.g., *Searle*, 1996; *Robinson*, 2009] and the Kashgar-Yecheng Transfer System (KYTS) [see *Cowgill*, 2010; *Sobel et al*., 2011]. In the south, the Shyok suture marks the transition to the Kohistan and Ladakh island arcs (Figure 1), which are, even further south, bounded by the continental suture between Eurasia and India (Indus-Yarlung suture or MMT), approximately 200 km south of our region of interest. Hence, the Pamir consists exclusively of material of Eurasian provenance [*Mechie et al*., 2012].

[6] North of the Pamir, the narrow Alai Valley separates the Pamir from the southern Tien Shan. It marks the last remnant of the former Tajik-Yarkand Basin and hosts at its southern margin the Main Pamir Thrust (MPT), where north-south convergence in front of the advancing Pamir is currently accommodated [*Coutand et al*., 2002; *Arrowsmith and Strecker*, 1999; *Zubovich et al*., 2010].

3. Data

[7] As part of the TIPAGE (TIen Shan PAmir GEodynamic Program) project, a total of 40 seismic stations,

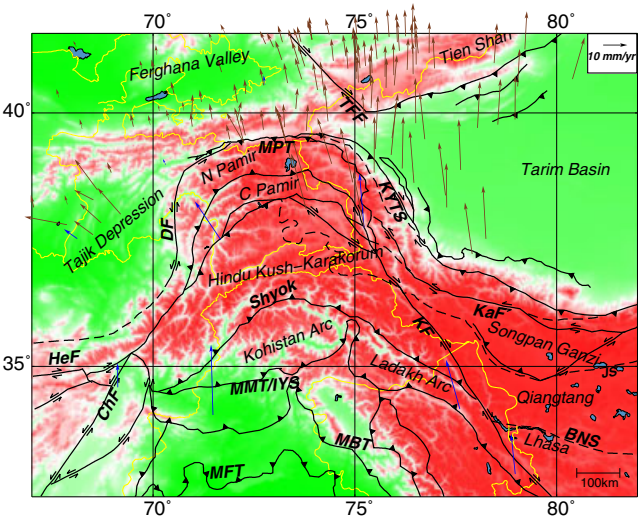

Figure 1. Topographic map of the study region, showing GPS velocities (brown arrows from *Zubovich et al.* [2010], and blue arrows from *Mohadjer et al.* [2010]) and tectonic features (faults and sutures) in the region, taken from *Robinson et al.* [2004] and *Mechie et al.* [2012]. HeF = Herat Fault, ChF = Chaman Fault, MFT = Main Frontal Thrust, MBT = Main Boundary Thrust, MMT/IYS = Main Mantle Thrust/Indus-Yarlung Suture, DF = Darvaz Fault, MPT = Main Pamir Thrust, TFF = Talas Ferghana Fault, KYTS = Kashgar-Yecheng Transfer System, KF = Karakorum Fault, KaF = Karakax Fault, BNS = Bangong Nujiang Suture, and JS = Jinsha Suture.

32 of them broadband sensors, were installed in southern Kyrgyzstan and eastern Tajikistan for a total duration of two years, from August 2008 to June 2010. The geometry of the array was changed in mid term, from a dense 24-station north-south profile with the other 16 stations distributed rather sparsely around it to a purely 2-D geometry evenly covering the whole region of interest (Figure 2). This network was complemented by two further temporary deployments: 21 broadband stations distributed around the Ferghana Valley, south-western Kyrgyzstan, from September 2009 to September 2010 [*Haberland et al.*, 2011], and seven short-period stations in the Alai Valley deployed for approximately 6 months soon after the 5 October 2008 Nura earthquake (M_w 6.6) for better coverage of aftershock seismicity. All temporary stations recorded continuous data streams at 100 Hz sample frequency. Additional data from several permanent networks in the region were retrieved through collaborations with various institutes and from online resources (www.iris.edu, geofon.gfz-potsdam.de), extending and densifying the network to cover all of Tajikistan and most of Kyrgyzstan. Although we analyzed the data and seismicity from the entire footprint of this extended network (Figure 2), we concentrate here on the results for the Pamir-Hindu Kush region.

4. Automatized Processing of Local Seismicity Data

[8] The rate of seismicity in our study region during the recording time was so high that conventional processing, i.e., locations based on manual phase picks, would only have allowed analysis of a subset of events. However, as one of the goals of this study is to present a realistic and as complete as possible image of the overall seismicity, we implemented an automated multi-stage processing chain for picking, locating and relocating earthquakes (section A). We used first detections from a short-term versus long-term average ratio (STA/LTA) trigger and a grid search algorithm for event association and preliminary locations (section A1), and then specialized *P* and *S* phase pick algorithms on targeted phase windows for an improved set of phase picks (sections A2 and A3), which were jointly inverted for new hypocenters, station-phase terms, and a 1-D velocity model (section A4). We finally calculated differential traveltimes based on waveform cross-correlation that were used together with phase picks in double-difference relocation (section A7). At each step, quality checks were implemented to weed out spurious picks, wrong associations, and false and badly constrained events. The complete catalog is supplied as an electronic supplement to this article. The successive improvement of event locations through the procedure leads to a sharpening of imaged structures, as illustrated in Figure 3.

5. Location Uncertainty

[9] To acquire a measure for the accuracy of our locations, especially with respect to network geometry, we employed a probabilistic relocation scheme of the events [*Lomax et al.*, 2000]. Here a probability density function (PDF) for the location of each single event is retrieved, together with an error ellipse containing 68% of this PDF. To visualize location uncertainties for this large three-dimensional data set, we subdivided the study region into three depth layers (0–70 km, 70–150 km, and >150 km) and each depth layer into 0.25°*0.25° bins. We then calculated the mean length of error ellipses for all events within each bin in longitudinal, latitudinal, and vertical directions. If a bin contained less than five events, it was left blank. The results of this computation are shown in Figure 4. It is discernible that the vertical error is in all cases larger than the horizontal errors and that shallow- and intermediate-depth events in the Hindu Kush have a rather bad depth resolution, whereas the deep ones are substantially better constrained. Throughout the Pamir, horizontal errors lower than 7.5 km and vertical errors lower than 15 km are found. Intermediate-depth events in the Pamir show better constrained focal depths than crustal events. It should be mentioned that there are secondary effects influencing the observed accuracy as displayed in Figure 4. If events in one bin, for example, are relatively small in magnitude, hence only have fewer constituent picks than events elsewhere, this will lead to a worse accuracy estimate than in a region which has comparable network geometry but larger (better picked) earthquakes.

[10] Uncertainties obtained in this manner estimate absolute location errors. Since, however, a relative double-difference relocation technique was used to determine the final hypocenters, relative location errors that would affect the shape of the imaged structures, not only their absolute positions, should be substantially lower than these values (see Section 7).

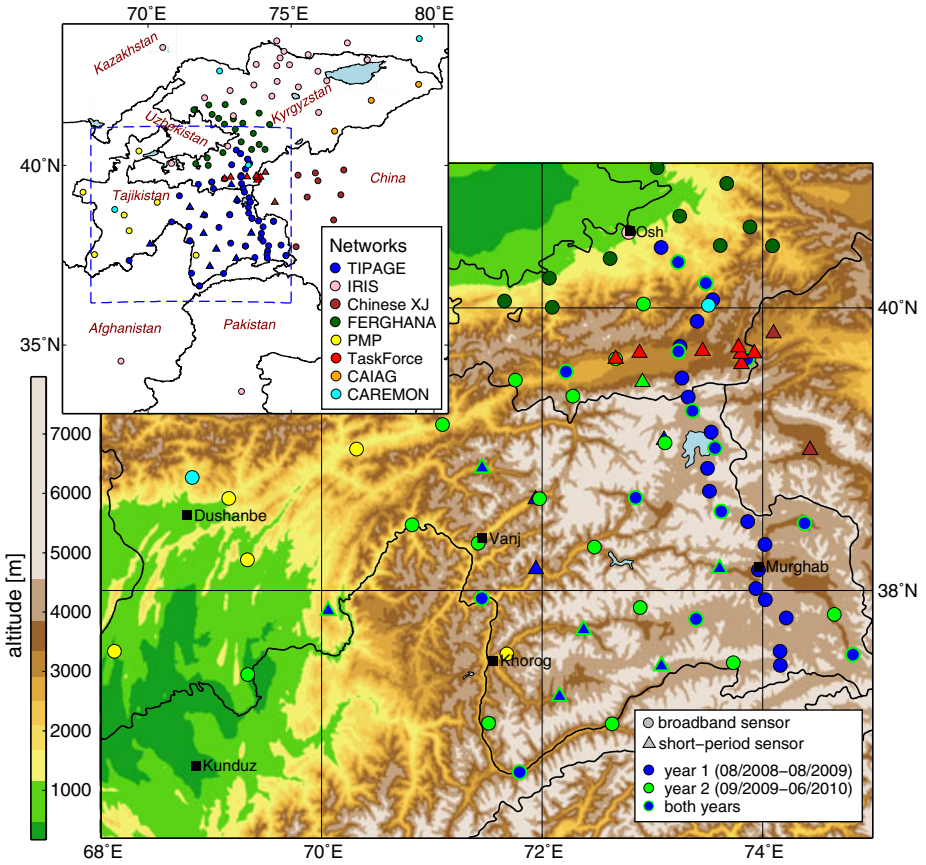

Figure 2. Map showing the distribution of seismic stations during both periods of the TIPAGE deployment (main figure) and the auxiliary stations that we utilized (upper left subfigure). The blue dashed box in the upper left subfigure marks the area shown in the main figure.

6. Results

[11] The seismicity in the earthquake catalog produced as described in section 4 and the Appendix is shown in map view and two projections onto a single longitudinal plane and a latitudinal plane, respectively, in Figure 5. Although there is abundant shallow seismicity, the S-shaped belt of intermediate-depth seismicity from the Hindu Kush in the

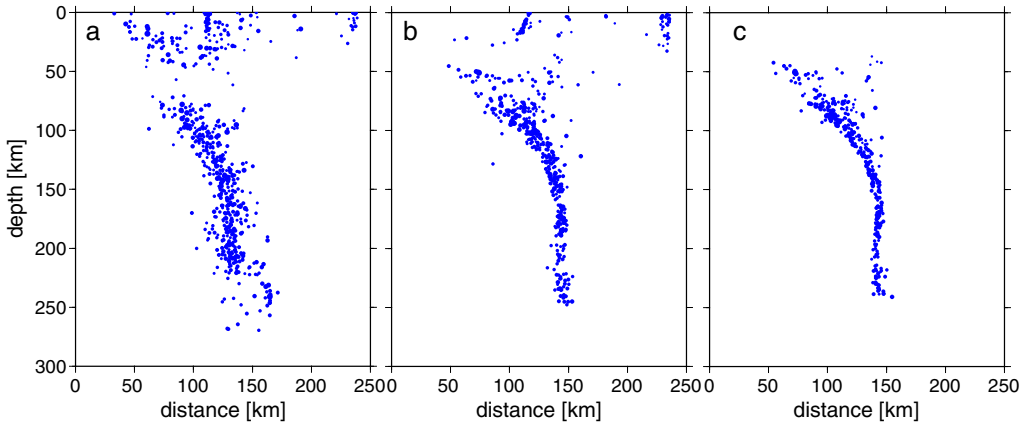

Figure 3. Comparison of an example profile (equal to profile E-E' in Figure 7) through the obtained earthquake location processing chain. (a) single-event relocation after *S* picking; (b) relocation with minimum 1-D model and station corrections; (c) double-difference relocations with catalog and cross-correlation derived differential arrival times. Only deep events are shown in Figure 3c, since not all distributed shallow events could be relocated with the double-difference method. Locations collapse to a more sharply defined structure from left to right.

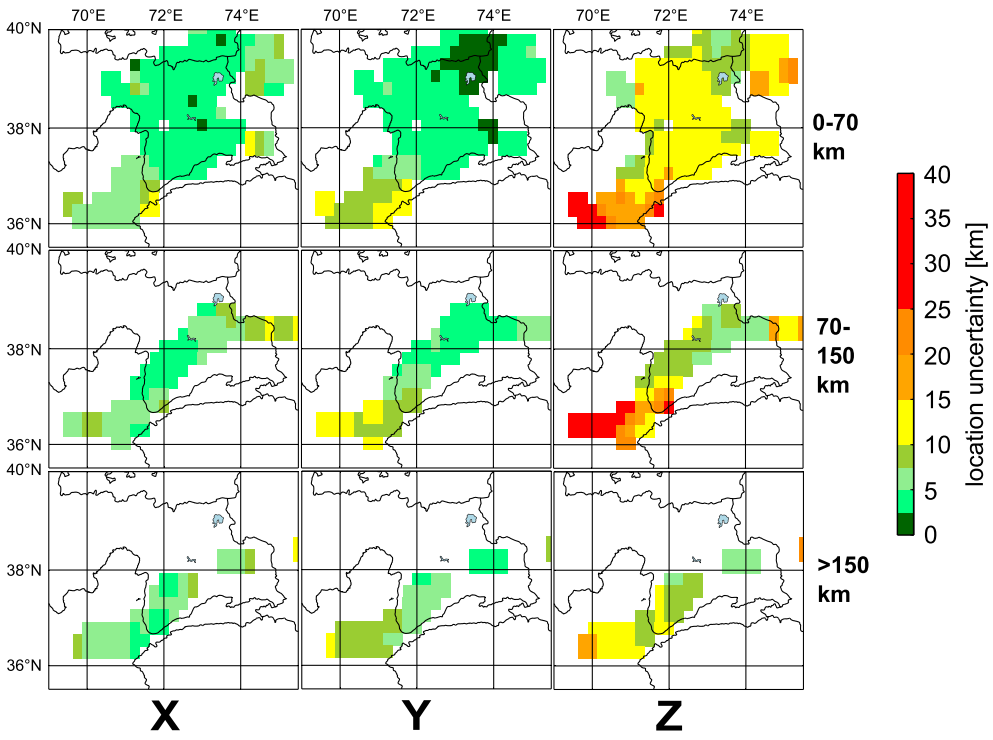

Figure 4. Mean location uncertainty, i.e., extent of the error ellipsoid, in longitudinal, latitudinal, and vertical directions calculated for 0.25°*0.25° bins in three depth layers, indicated at the right of the images. Bins containing less than five earthquakes are left blank.

southwest to the eastern Pamir is the most prominent feature on the map. The massive curtains of deep earthquakes seen in the vertical sections will be untangled based on narrower vertical profiles in the following.

6.1. Shallow Seismicity

[12] The distribution of seismicity with hypocentral depths shallower than 50 km (crustal) is shown in Figure 6a. Most shallow-focus earthquakes in our dataset are located at the northern circumference of the Pamir, at or south of the southern margin of the Alai Valley, where the MPT surfaces. The strong cluster of seismicity in the eastern part of the Alai Valley originated mostly from the aftershock activity associated with the October 5, 2008 Nura earthquake (M_w 6.6). While crustal seismicity in northern and western Tajikistan, particularly in the Garm region, has been studied extensively during Soviet times [e.g., *Nersesov and Semenov*, 1969; *Konopaltsev*, 1970; *Martynov et al*., 1976; *Eneva et al*., 1992], far less is known about crustal seismicity in the Pamir mountains. In our dataset, the eastern Pamir plateau appears to be largely aseismic, whereas the deeply incised western Pamir shows several seismically active zones. A northeast-southwest striking lineament passing lake Karakul in the north appears to separate these two regions. Crustal seismicity is concentrated in the uppermost 25 km (see Figure 5 and profiles in Figure 7), and middle to lower crustal levels appear to be aseismic. The correlation of shallow seismicity to mapped geological structures is beyond the scope of this paper.

6.2. Intermediate-Depth Seismicity

[13] The geometry of structures outlined by intermediate-depth earthquakes in the Pamir and Hindu Kush is shown in a series of representative profiles (Figure 7) and depth maps (Figure 6). We distinguish two distinct zones of seismicity—the Pamir and the Hindu Kush seismic zones—separated by a seismic gap and a 90° change in dip and strike directions around 36.8°N, 71.4°E, discussed in more detail below.

6.2.1. Pamir

[14] The Pamir seismic zone begins at the boundary of the Pamir with the Tarim Basin in the east and ends slightly northeast of the Hindu Kush zone's eastern termination, dipping due east (see cross-section E-E', Figure 7). Intermediate-depth earthquakes in this zone are confined to a thin (about 10–15 km thick), curviplanar structure outlining an arc, with its strike gradually changing from north-south to east-west and the dip changing from eastwards to southwards (see profiles E-E' through I-I' in Figure 7). All along this arc, the dip angle stays approximately constant at around 50°, except for depths greater than 150 km in the western part of the structure, where the dip steepens to become (sub)vertical (see profiles E-E' and F-F'). Some uppermost mantle earthquakes in these two profiles are located southeast or east of the curved plane defined by the majority of events. They appear to form a structure resembling a backthrust in a hanging wall (see profiles E-E' and F-F' in Figure 7).

[15] Intermediate-depth seismicity in the Pamir is separated from shallow crustal activity by an apparently largely aseismic lower crust (depth region 25–70 km).

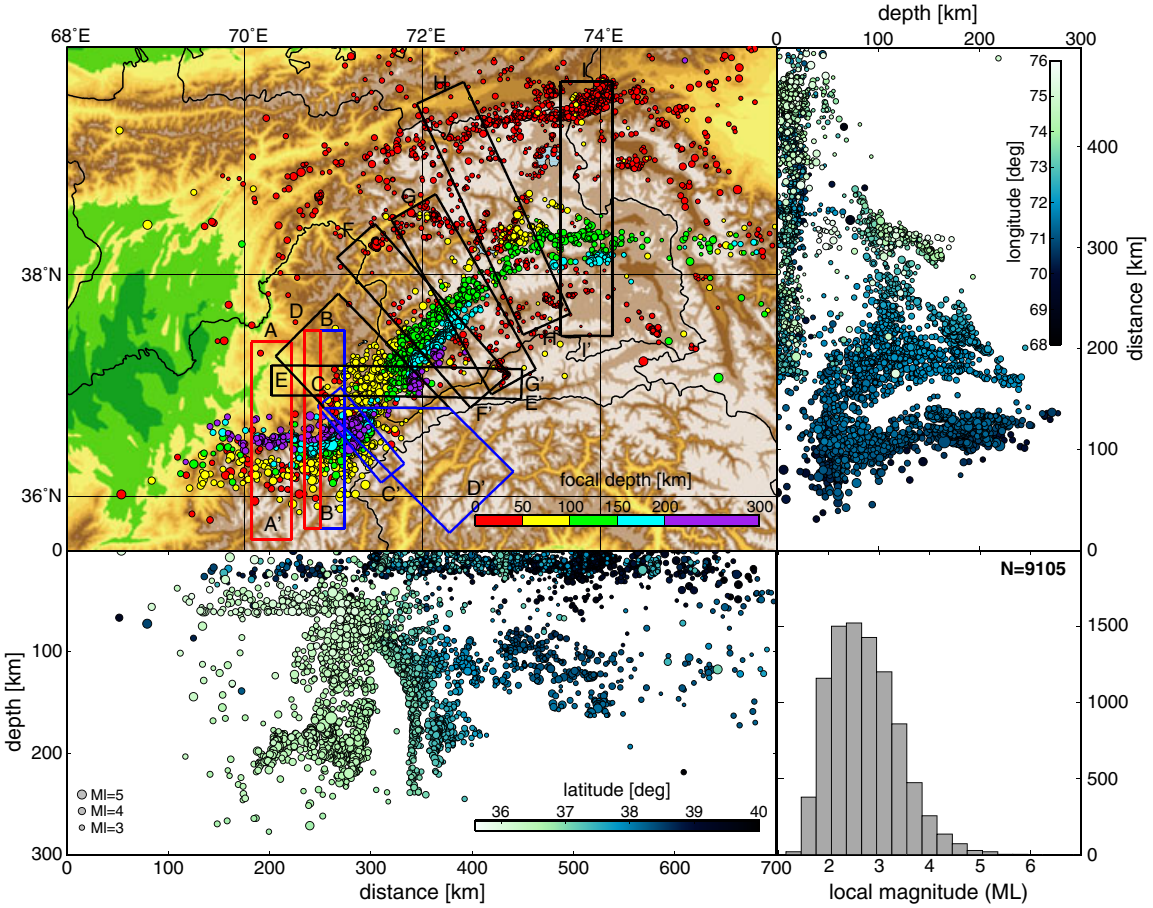

Figure 5. Overall distribution of seismicity in the study area from August 2008 to June 2010 in map view (plotted onto a topographic map) and as projection of all events onto a longitudinal and latitudinal plane. Dot sizes denote different earthquake magnitudes, and colors denote different depth levels (in the map view plot) and distance from the projection plane, respectively, as indicated in the color legends. Deeper events were plotted on top of shallower ones in the map view subplot, nearer events on top of farther ones in the projections. Boxes indicate the location and extent of the profiles shown in Figure 7; colors reflect a subdivision in western Hindu Kush (red), eastern Hindu Kush (blue), and Pamir (black), which is reflected in the colors in Figure 7. Lower right sub-figure shows the distribution of local magnitudes in our data set. A total of 9105 of the total number of 9532 earthquakes are shown here; the missing events are located north of the region shown in this plot.

Earthquakes in the Pamir deep seismic zone are located at depths greater than about 70 km. Their deepest extent is 170 km in the eastern part of the zone and 250 km in the zone's western part. These deepest earthquakes in the western Pamir form two subparallel, vertical "streaks" as evident from Figure 6e. A gap in seismicity at 150–200 km depth (Figure 6d) around 73°E marks a zone where the maximum depth and the density of earthquakes reach a minimum; further east, greater depths are reached again toward the zone's termination (see also color-coded stripes in Figure 5). Towards its southwestern end, the Pamir seismic zone abruptly changes its strike (best visible in Figure 6d), from NE-SW to due north-south. Local magnitudes in the Pamir seismic zone are generally moderate to low during our recording period, with only a handful of events stronger than M_L 4.5.

6.2.2. Hindu Kush

[16] The Hindu Kush seismic zone is generally oriented east-west at roughly 36.4°N, with a sharply defined eastern end toward 71.4°E and a less clear western end somewhere between 69° and 69.5°E (Figure 5). Hypocenters extend in depth from roughly 40 to 250 km, with only a few isolated earthquakes outside this depth range. Cross sections (Figure 7, profiles A-A' to D-D') and depth cuts (Figure 6) reveal significant geometric complexity.

[17] In its westernmost part (Figure 7, profile A-A'), earthquakes in the Hindu Kush are confined to a tight cluster at 180–220 km depth that dips steeply southward. This cluster shows a northward convex curvature along strike, as visible in Figure 6d, and appears to be unconnected to some diffuse seismicity at lower crustal or uppermost mantle depths shown in the same profile. The termination of this part of the Hindu Kush can be seen in a change in strike and dip directions around 70.85°E, towards a more planar, WSW-ENE trending and steeply northward dipping structure east of this longitude (Figure 7, profile B-B'). The transition between these two zones is apparent as a southward protruding spur in Figure 6d.

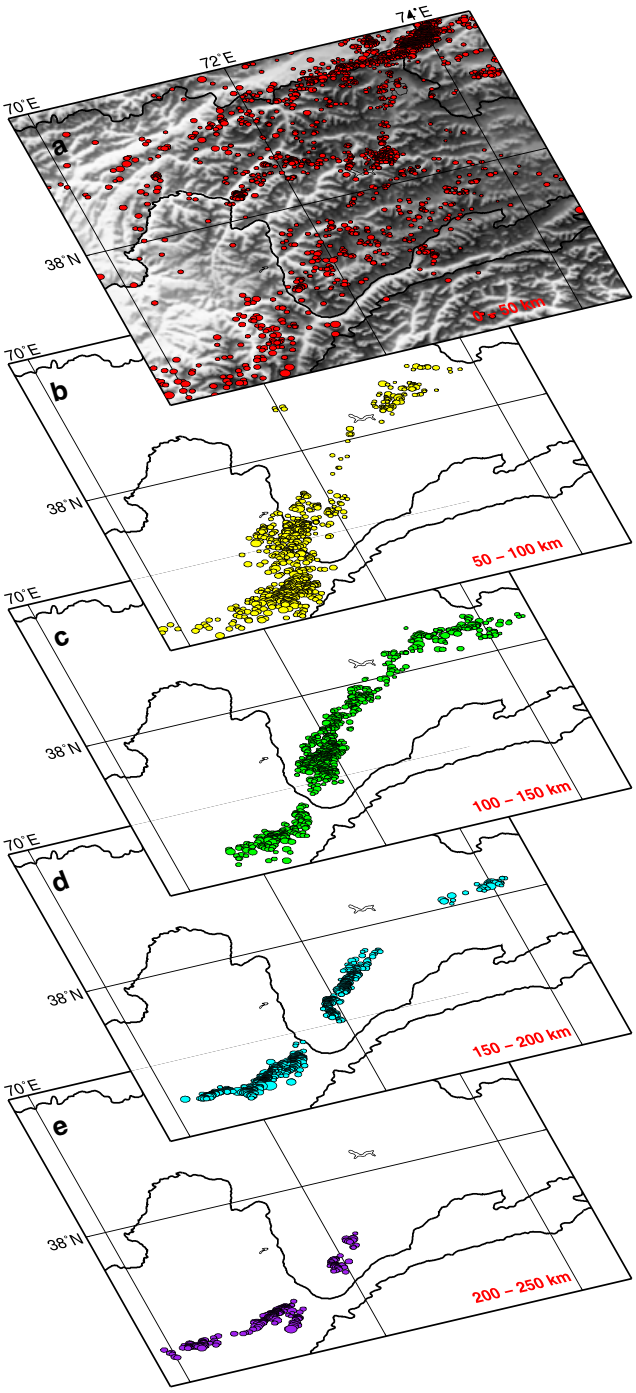

Figure 6. Depth cuts through the study region—all earthquakes from one depth bin (extent indicated at the lower right of each map view plot) are projected onto a horizontal (map view) plane. Color scheme identical to Figure 5, map view plot. Black lines indicate national boundaries.

[18] In the eastern part of profile B-B' (blue earthquakes), earthquake hypocenters outline a more planar structural entity extending from crustal depths to about 250 km depth. Most seismicity is concentrated between 160 and 210 km depth, whereas nearly no earthquakes are observed directly above this. For the whole structure, a slight northward dip is discernible, although this inference is less robust for its shallower part, due to the greater scatter in earthquake locations observed here, likely owing to lower location accuracy (section 5). Still further east (profile C-C'), the Hindu Kush seismic zone's strike progressively bends toward a NE-SW direction, aligning with the general strike of the Pamir seismic zone, and there is a clear segmentation into an upper and a lower part, separated by a seismic gap at 150 km depth. To the shallow side of this divide, hypocenters outline a planar feature dipping northwestward. Below 150 km, a subdivision of the structure into three separate earthquake clusters is discernible. The exact geometric configuration of these clusters is complex and difficult to comprehend at first glance and might need some immersion into the profiles and depth maps. The shallowest of these deep clusters extends from 150 to about 200 km depth and appears to be continuous with the shallower part both in dip direction and width. Below 180 km depth, two parallel striking clusters frame the first one on both sides, i.e. northwest and southeast of it. At depths greater than 200 km, where the uppermost of the three clusters is not observed any more, these parallel clusters are horizontally separated by about 15 km, which leads to the pattern of two parallel streaks in the depth map (Figure 6e) and to an inverted-V or fork-like appearance in the profiles (Figure 7, profiles C-C' and D-D'). Whereas the two lowermost clusters are planar with a considerable horizontal extent, the shallowest of the three clusters is only present in the direct vicinity of the Hindu Kush zone's eastern termination, its shape resembling a narrow finger.

[19] Profile D-D', which images earthquake hypocenters to both sides of the gap separating the Pamir and Hindu Kush seismic zones, shows the jump in dip occurring across this gap. Whereas there is a clear change in dip polarity at levels shallower than 150 km, the structures apparently align in their lower parts, where both are sub-vertical. This alignment, however, can only be observed for the uppermost of the three deep clusters in the eastern Hindu Kush, whereas Hindu Kush and Pamir seismicity again diverges below 200 km depth. One should, however, look at this projection with some caution, since the southwesternmost Pamir is not projected onto a plane perpendicular to its strike (which is north-south). Hence, the discrepancy of dips imaged here appears to be smaller than it really is. Inspection of profiles E-E' and C-C' and their map view location gives a more accurate picture of the change in vergence across the gap.

[20] Seismic moment release is significant in the Hindu Kush, with 81 earthquakes of $M_L > 4.5$ (of a total of 138 for the whole study area) present in our 2 years' data. A large majority of the bigger earthquakes occurs in the deeper clusters, i.e., below the vertical gap at approximately 150 km. The thickness of the planes defined by the hypocenters is around 15–20 km (see profiles in Figure 7), only slightly thicker than for the Pamir. Seismic activity in the Hindu Kush zone is confined to mantle and possibly (high location uncertainty for shallowest part; Figure 4) lower crustal depths. No connection to shallow crustal activity is evident.

7. Discussion

[21] A vast majority of the observed intermediate-depth seismicity occurs in clusters that reveal clearly planar structures of limited thickness (10–15 km) at suitable cross-section angles (Figure 7). A schematical interpretation of the

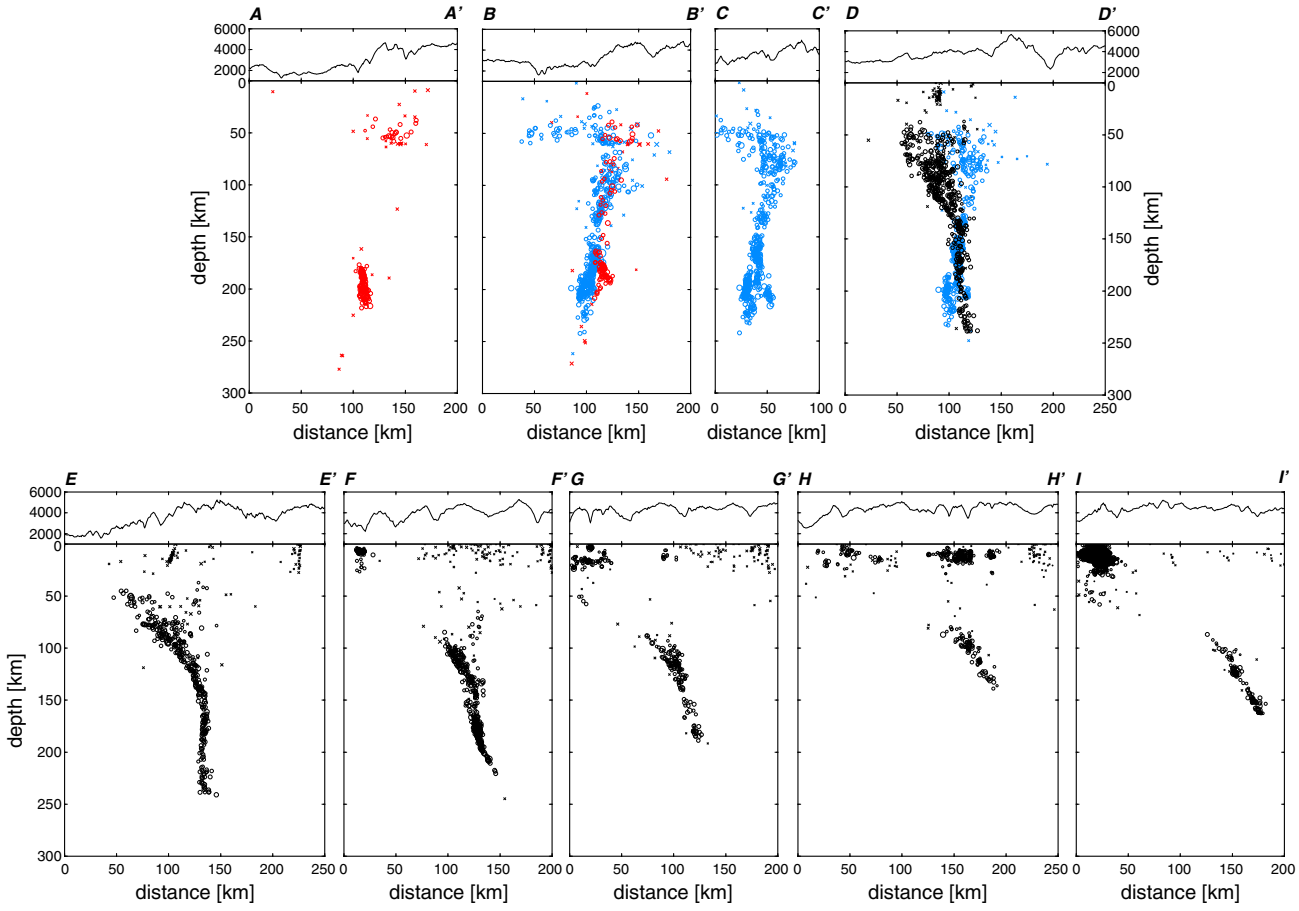

Figure 7. Series of profile projections perpendicular to the strike of the structure outlined by intermediate-depth earthquakes in Pamir and Hindu Kush. Locations of the profiles are indicated in Figure 5. Average topography across the swath widths is shown on top of the profiles. Circles denote earthquakes relocated with the double-difference method; crosses are events where this relocation was not performed. Colors of earthquake markers refer to different structural units (red: western Hindu Kush, blue: eastern Hindu Kush, and black: Pamir) and are likewise indicated in Figure 5.

configuration of these planes is sketched in Figure 8. The first-order division of seismicity into the Pamir and Hindu Kush seismic zones can be performed across a clear gap in seismicity coincident with a change in dip direction of the Benioff zone. This gap tapers off towards shallow depths, where both zones adjoin close to the presumed Moho position. The Pamir can be interpreted as a single curved plane, with its curvature and vertical extent increasing toward the southwest. Along with the change in strike from east-west to north-south, the dip direction changes from due south to due east at its south-westernmost termination, where it meets the Hindu Kush. The Hindu Kush zone is much more compact compared to the Pamir zone. To first order, it strikes east-west and bends northward at its eastern end to converge with the general trend of the western Pamir zone. Hindu Kush seismicity appears to be separated into an upper and lower part by a vertical gap at approximately 150 km depth. The upper part of the Hindu Kush seismicity is quite sparsely sampled yet reveals a steep north to north-westward dip. The lower part of the zone consists of a number of highly active clusters that form a complex mosaic of several steep planes of variable size, strike, dip direction, and curvature.

[22] Before any interpretation attempt, we have to consider the possible influence of location uncertainties on our shown results. Absolute location error estimates from probabilistic relocation (section 5) are variable throughout our study region, with small to moderate values for most of the Pamir (less than 10 km except for the depth of shallow events) and significantly higher values (up to 35–40 km vertical uncertainty) in the Hindu Kush, which is situated outside of our station network (Figure 4). These errors represent the effects of data noise, picking errors, and event-station geometry but not of errors due to deviations of the used velocity model from real earth structure. The fact that double-difference relocations collapse to structures rarely exceeding a width of 10 km in the Pamir (Figures 3 and 7) and 15 km in the Hindu Kush, however, shows us that relative location errors have to be substantially smaller. If we assume that relative location errors are random, the half-width of these structures, 5 and 7.5 km, respectively, can be used as a maximum estimate for relative location uncertainties. The largest uncertainties are present for relatively shallow-focus events in the (western) Hindu Kush, where even double-difference relocations do not outline

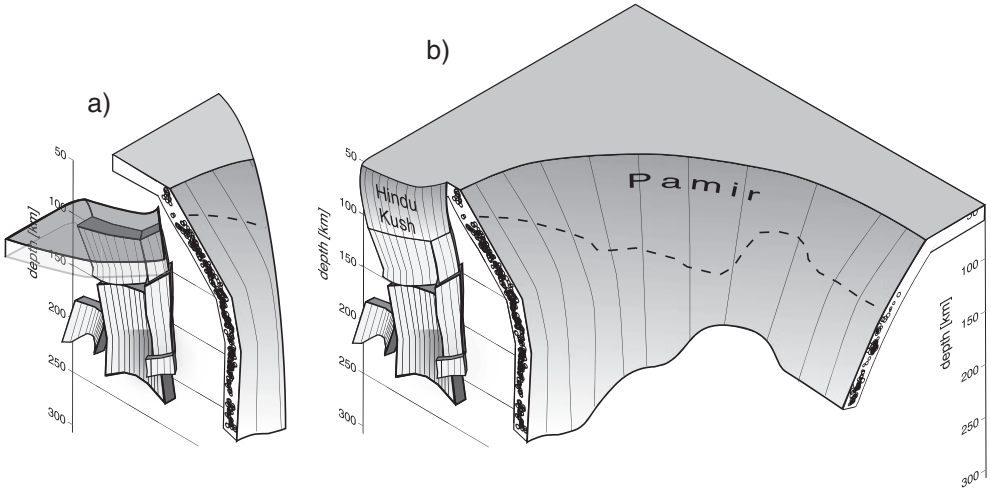

Figure 8. Schematic representation of the geometry outlined by the earthquake locations presented in this study. The Pamir seismic zone defines an arc which incrementally changes its dip direction from southward to eastward and its strike direction from east-west to north-south from east to west. Dashed line corresponds to the upper limit of intermediate-depth seismicity along strike. The Pamir's dip angle stays constant along strike at depths shallower than 150 km. Southwest of the Pamir arc, clearly separated from it in terms of dip direction, is the Hindu Kush seismic zone, which strikes roughly east-west and generally dips nearly vertically northwards. A tendency toward a strike alignment with the western Pamir is discernible in its eastern part. Although significantly smaller in width, the Hindu Kush exhibits considerably more structural complexity than the Pamir, shown by its fragmentation in several (curvi)planar fragments.

sharply defined structures but a relatively diffuse cloud of hypocenters. Manually locating earthquakes in this region, we experienced quite unstable hypocentral depths due to an unfavorable network geometry. We think that the cloud of seismicity we image at lower crustal depths in the western and central Hindu Kush most likely represents mislocated upper crustal seismicity. We thus conclude that the imaged geometries should be robust (error no larger than 5–7.5 km), with the possible exception of Hindu Kush seismicity shallower than about 100 km. The errors in the absolute position of these features, however, may be substantially larger. The retrieved catalog should be quite comprehensive, i.e., not many events should have been missed, for at least M>2.5 in the Pamir and M>3.5 in the Hindu Kush (varying with the station coverage). An exception to this is western Tajikistan, where we fail to detect some crustal earthquakes in the event association step, due to inappropriateness of our averaged velocity model for the Tajik Depression with its thinner crust compared to the Pamir and its thick (up to 10 km) sedimentary layer. Hence, crustal seismicity plotted in Figure 5 for western Tajikistan is most likely underestimated.

7.1. Processes Responsible for Intermediate-depth Seismicity

[23] It seems manifest that the intermediate-depth seismicity beneath one of the most active orogens on Earth attests to active deformation in the sub-crustal lithosphere. The mode of convergence and the resulting deformation pattern at depth as well as the ultimate fate of the lithosphere(s), however, are not well understood. As crust is shortened and thickened, the underlying mantle lithosphere might either detach from the crust and subduct on one side of the orogen, or it might likewise thicken through simple shear underthrusting or pure shear shortening. During the latter process, thickened lithosphere might become gravitationally unstable [*Leech*, 2001] and delaminate as an intact sheet [*Bird*, 1979] or viscously drip into the underlying asthenosphere as a Rayleigh-Taylor instability [*Houseman et al.*, 1981]. All these processes have been suggested to occur in the Indo-Eurasian collision zone [e.g., *Tilmann et al*., 2003; *Nábelek et al*., 2009; *Koulakov*, 2011]. It is not easy to distinguish between them, because mantle images from teleseismic waves are often too fuzzy and inferences from surface observations, like uplift history and magmatism, are non-unique. Based on the visual appearance of a drop-like high seismic velocity anomaly that reaches all the way into the mantle transition zone beneath the Hindu Kush, *Koulakov* [2011] suggested a lithospheric drip currently occurring there. It is not clear whether a Rayleigh-Taylor instability, which is a ductile process, would be capable of creating any seismicity at all. Indeed, well-constrained mantle downwellings beneath Tibet [*Tilmann et al.*, 2003], the Andes [*Schurr et al.*, 2006], the Colorado plateau [*Levander et al.*, 2011], and the Sierra Nevada [*Zandt et al.*, 2004] take place aseismically. *Lorinczi and Houseman* [2009] could reproduce strain rates measured for the Vrancea intermediate-depth seismic zone by numerically simulating a narrow lithospheric downwelling. In their model, deformation is not localized, but distributed within the drip. Our observation that Pamir-Hindu Kush seismicity is highly localized along well-defined thin planar structures is difficult to reconcile with any such process but rather evokes one that involves plunging plates like subduction or sheet-like delamination.

[24] Intermediate-depth seismicity occurring dominantly in thin planes hints at the existence of a lithologically and/or rheologically distinct layer where conditions allow brittle

material failure. In a chemically more or less homogeneous mantle, earthquake occurrence should be controlled by pressure and temperature alone, which would make it difficult to account for both the concentration of earthquakes in a thin layer and its depth span exceeding 200 km. The variability of source mechanisms in the Pamir and Hindu Kush zones [*Pegler and Das*, 1998; *Lister et al.*, 2008] also speaks against the possibility that earthquakes mark a localized mantle shear zone. Instead, we prefer the interpretation that earthquakes occur in a crustal layer that is entrained in the mantle. This is supported by the observation that intermediate-depth seismicity emanates near the presumed Moho depth, at least in the western Pamir and Hindu Kush. The similarity of the Pamir-Hindu Kush earthquakes to inclined Wadati-Benioff zones known from oceanic subduction and source mechanisms exhibiting down-dip extension (at least beneath the Hindu Kush), also a hallmark of intermediate-depth earthquakes in oceanic plates, early on led to the belief that they are the expression of subduction of a last piece of the Neo-Tethys Ocean or another remnant ocean basin [*Chatelain et al.*, 1980]. However, Pamir and Hindu Kush are far beyond the Indus-Yarlung suture (Figure 1) where oceanic subduction is supposed to have stopped with the arrival of continental India. There is no indication of the subduction of a possible land-locked ocean basin north of the suture in the regional rock record [*Burtman and Molnar*, 1993], and the absence of large-scale Cenozoic volcanism seems to confirm this [*Schwab et al*., 2004]. If we thus discard the possibility of subduction of a remnant ocean basin beneath the Pamir and note that subduction of oceanic material from the south should have stopped not later than 40 Ma ago [*Yin and Harrison*, 2000], this rules out the presence of oceanic material at depth. Earthquakes would hence trace continental crustal material on top of a mantle lithospheric slab. *Roecker* [1982] observed anomalously low seismic wave speeds co-located with intermediate-depth seismicity in the Hindu Kush with local earthquake tomography and interpreted these findings with the presence of continental crustal material at depth. Such a presumably small-scale anomaly would likely not be resolved by the regional or global tomographic models of *Koulakov and Sobolev* [2006], *Koulakov* [2011] and *Negredo et al.* [2007], which only image the deeper, larger-scale structures. Presence of continental crust at mantle depths (65–110 km) is also supported by crustal xenoliths erupted at 11 Ma in the south-eastern Pamir [*Ducea et al*., 2003; *Hacker*, 2005; *Gordon et al*., 2012]. The observed layer thicknesses of 10–15 km imply that only a part of the continental crust would be involved, which is consistent with the argumentation of *Molnar and Gray* [1979] that deep subduction of continental lithosphere, due to its higher buoyancy, should only be possible if the upper crust is scraped off and stays at the surface.

[25] The inference that intermediate-depth earthquakes occur within subducting or delaminating continental lower crust, however, does not immediately solve the problem of seismogenesis. The most frequently evoked model for the generation of intermediate-depth earthquakes in oceanic subduction zones is dehydration embrittlement [*Kirby et al.*, 1996; *Hacker et al.*, 2003; *Hacker*, 2003; *Jung et al.*, 2004], which allows rapid shear failure in a pressure and temperature regime where rocks would otherwise deform in a ductile manner. In this conceptual model, fluids released in prograde metamorphic reactions from hydrated minerals reduce normal stress and friction in the surrounding material and thereby enable brittle fracture and slip that would otherwise be inhibited by the high confining pressure at depth. However, lower continental crustal rocks do not typically contain any significant amount of hydrated minerals [*Rudnick*, 1995; *Rudnick and Fountain*, 1995] and should therefore predominantly deform aseismically at mantle depths. In a delamination scenario for the Pamir, the southern and central Pamir's origin from accreted volcanic arcs [*Schwab et al*., 2004] may provide preserved fluid reservoirs in hydrated rocks that are now released as these rocks are transported to greater depth. Alternatively, concepts of shear instabilities by thermal runaway [*Kelemen and Hirth*, 2007; *John et al.*, 2009] have been proposed for the generation of intermediate-depth earthquakes. Invoking these concepts, one could speculate that existing fine-grained shear zones in the lower crustal material, which are necessary for strain localization, might constrain earthquakes to the crustal layer. In any case, it remains an open question what the predisposing factors and specific processes are that cause the virile deep seismicity in an intra-continental setting that is observed almost nowhere else.

7.2. Provenance of Imaged Structures—Eurasia or India?

[26] The peculiar geometry of the two Benioff zones apparently dipping in opposite directions invariably leads to the question of their provenance. There are essentially two prevailing lines of interpretation in the literature: (1) Both Pamir and Hindu Kush slabs belong to a single slab of Indian origin which is torn, contorted and overturned in its south-dipping Pamir part [*Billington et al.*, 1977; *Pegler and Das*, 1998; *Pavlis and Das*, 2000]. (2) Pamir and Hindu Kush are two distinct slabs subducting in opposite directions next to each other, where the Pamir slab is made up of Eurasian material and the Hindu Kush slab is of Indian provenance [*Burtman and Molnar*, 1993; *Fan et al.*, 1994]. Alternatively, a two-slab model involving the subduction of two remnant oceanic basins (which would have to be embedded in Eurasian lithosphere) in opposing directions has been proposed by *Chatelain et al.* [1980]. This last possibility, however, appears to us highly ad hoc and not compatible with available surface evidence.

[27] The geometry of the Pamir slab imaged here, with its clear separation from the Hindu Kush and general south- to southwestward dip, seems hard to reconcile with any process involving Indian material, but instead strongly suggests to us a Eurasian origin. A hypothetical plane through the intermediate-depth seismicity below the eastern Pamir projected updip would emerge near the MPT (Figure 7, profile I-I'). The MPT separates the intermontane Alai valley, probably the last remnant of the Tajik-Yarkand Basin, from the over 7000 m high Trans-Alai Range at the Pamir's northern deformation front. The MPT is seismically active (see Figure 6a), and a convergence rate of 10–15 mm/yr across it is constrained by GPS measurements [*Reigber et al*., 2001; *Zubovich et al*., 2010]. The deep Pamir seismic zone could be seen as the continental analog to a highly arcuate, narrow subduction zone segment like the Caribbean or the Banda Arc ones [*Spakman and Hall*, 2010]. In such

a model, the arcuate shape of the Pamir seismic zone would be the consequence of the shape of the Indian indenter further south (western syntaxis), which led to the creation of northward-convex structural belts throughout the orogen and the arcuate Pamir deformation front and slab. The prevalence of along-arc extensive mechanisms of intermediate-depth earthquakes beneath the Pamir, which *Pegler and Das* [1998] used as an argument in favor of active contortion of a single seismic zone of Indian origin, could be reconciled with such a purely Eurasian Pamir seismic zone in combination with active slab rollback [*Sobel et al.*, 2013]. The MPT would mark the intersection of the plate interface with the surface and the strike-slip faults at the Pamir's edges (Darvaz/Chaman Fault and Karakorum Fault/KYTS) would accommodate northwards rollback of the whole system as so-called STEP faults [see *Govers and Wortel*, 2005]. Scraped-off upper crustal material from the downgoing slab would form the imbricate thrust sheets making up the Trans Alai. An alternative model resulting in the same observed geometry beneath the Pamir would be one that invokes delamination. In that scenario, lithosphere beneath the Pamir would have thickened through its overthrusting onto the Tajik-Yarkand Basin to the point of becoming gravitationally unstable, when a sheet of lower crust and mantle lithosphere starts to peel off in a manner similar to what is suggested by analog [*Bajolet et al.*, 2012; *Chemenda et al.*, 2000] and numerical [*Bird*, 1979; *Gögüs and Pysklywec*, 2008] simulations. The clear gap between shallow seismicity at the MPT and sub-crustal earthquakes would then separate different active processes. Lithosphere delaminating along an arcuate hinge would also naturally experience horizontal tensional stresses in the slab in accordance with observations. Although implying a distinctly different evolutionary history of the whole orogen, such a scenario could lead to the same temporal snapshot we image today.

[28] The Hindu Kush seismic zone's general northward dip direction provokes an association with Indian material. Since the involved material is most likely of continental origin (see argumentation above), the underthrusting of continental India beneath Eurasia, occurring in along-strike continuity of active processes in the Himalayas and beneath the Tibetan Plateau [e.g., *Yuan et al*., 1997; *Kosarev et al*., 1999; *Kind et al*., 2002; *Nábelek et al*., 2009; *Kind and Yuan*, 2010], could provide the host material for Hindu Kush earthquakes [as first proposed by *Coward and Butler*, 1985]. Since its onset, the deformation front of the India-Eurasia collision has propagated southwards from the Indus-Yarlung Suture (Figure 1) to the MFT in the Indian plate. Thus, a substantial aseismic, sub-horizontal northward underthrusting of Indian lithosphere and lower crust at depth [which is observed in Tibet; see, e.g., *Li et al*., 2008; *Nábelek et al*., 2009] would be necessary for Indian material to reach the Hindu Kush, where seismicity and a seismic high velocity zone are observed today. Upon reaching the southern rim of the Tajik Depression, this lithospheric slab would have to steepen to near-vertical while starting to generate vigorous seismicity in its crustal part. Further east, there is no continuation of Hindu Kush seismicity, and an unimpeded northward propagation of underthrusting India would not be compatible with the presence of a Pamir slab. Hence, the deeper part of the Indian slab must have detached, whereas a remnant stub could still impinge onto the Pamir slab today, possibly causing its steep dip angle [*Fan et al.*, 1994]. A schematic representation of this concept is shown in Figure 8a.

[29] However, there are some observations that imply that the Pamir and Hindu Kush mantle earthquakes may occur under the same process, similar environmental conditions, or even in rocks of the same provenance. As described above, the gap separating the two zones is not complete but tapers toward shallower level until the earthquake zone becomes continuous close to the crust mantle boundary (Figure 6b). If viewed in perspective, this gives the impression that the earthquakes form a single curtain (rather than two) that is torn apart across the gap between Hindu Kush and Pamir (Figure 8b). Other clues that may support this interpretation are the alignment of strike of both Hindu Kush and Pamir seismicity across the gap (Figures 6c and 6d) and the significance of the 150 km depth level on both sides, where a break in seismicity or kink towards steeper dip is observed, respectively. Moreover, the simple fact that this globally almost singular seismicity would hardly be occurring fortuitously in two distinct structures next to each other may hint at a common origin.

[30] Following this interpretation, the Hindu Kush seismicity would have to be part of a larger Eurasian slab that is now slightly overturned, whereas the Pamir slab has been ripped away (Figure 8b). In such a model, the Indian slab would have had to be lost in order to make space for subduction of Eurasian lithosphere. A major break-off of the subducted Indian lithosphere has been suggested to have occurred 10–25 Ma ago [*Maheo et al.*, 2002; *Chemenda et al.*, 2000; *DeCelles et al.*, 2002].

[31] The western demarcation of the Pamir orogen in all likelihood reflects the westward extent of the Indian indenter further south, evident from the transition from collision tectonics in the Pamir to a predominance of strike-slip faulting throughout Afghanistan [*Tapponnier et al.*, 1981]. Along India's western flank, the lithosphere-scale Chaman Fault accommodates most of the relative motion between India and Eurasia. The more easterly surface boundary between Eurasian and Indian rock units only images thin-skinned deformation of sediments in the fold-and-thrust belts east of the Chaman Fault [*Haq and Davis*, 1997; *Bernard et al.*, 2000]. A hypothetical northeastward prolongation of the Chaman Fault would approximately line up with the western end of intermediate-depth seismicity in the Pamir-Hindu Kush, strengthening the argument that the slab width is defined by the lateral termination of India.

[32] We can only speculate what process could have caused the tear that separated the Pamir from the Hindu Kush in such a one-slab scenario. One candidate is the interaction of the slab with strong mantle lithosphere underlying the Tajik Depression. The Hindu Kush part of a formerly continuous slab might have been pinned against the southern rim of Tajik Depression lithosphere, whereas the Pamir part has been torn away by its continued northward advance. The imaged bends of both structures towards each other near their intersection (Figure 6d) would reflect processes directly before the tear took place, when the slab must have been stretched and contorted in the region around the locus of the final tear. With ongoing northward indentation of the Pamir, its deformation front and hence the hinge point of the subducting slab propagated north, developing

an arcuate shape that probably mimics the outline of the Indian salient further south. The intriguing alignment of intermediate-depth seismicity with surface features, with the Pamir deep seismic zone tracing the curvature of structural belts in the shallow Pamir and the Hindu Kush seismicity situated at the southern rim of the Tajik Depression, would be a consequence of this scenario. Moreover, the location of the seismic gap separating Pamir and Hindu Kush deep seismicity at the point where Pamir, Hindu Kush, and Tajik Depression meet, corresponds to what such a model would predict. This model would advocate that shallow and deep processes acting at the Pamir and Hindu Kush are coupled.

[33] In summary, based on our observations, we associate the Pamir zone of intermediate-depth earthquakes with a continental slab of Eurasian provenance, where the thin planar structure outlined by seismicity most likely represents lower crustal material. This inference leads us to exclude a one-plate model featuring a purely Indian slab. While we can not rule out a two-plate scenario, in which the Hindu Kush represents underthrusted continental Indian material, we currently prefer a one-plate model in which both Pamir and Hindu Kush deep seismic zones derive from a single Eurasian slab that is torn and overturned in its Hindu Kush part. Given that the occurrence of intermediate-depth seismicity in continental material in the Pamir-Hindu Kush is globally unique (section 1), it appears to us rather unlikely that two independent processes active next to each other by pure coincidence would both create these special earthquakes. However, only additional data, e.g., on stresses inside the seismic zones from earthquake mechanisms and possibly a three-dimensional seismic velocity model may allow us to better understand the geodynamic processes acting in this intriguing part of the world.

8. Conclusions

[34] Utilizing local seismic waveform data, we have developed an automatized processing chain for the retrieval of *P* and *S* arrival time picks and event locations. Obtained phase picks are shown to resemble manual picking in accuracy but not in hit rate. Event locations of 9532 earthquakes clearly show the presence of two distinct zones of intermediate-depth seismicity in the Pamir and Hindu Kush, separated by a seismic gap with a 90° discontinuity in dip direction across it. Earthquakes in the Hindu Kush to first order define an east-west striking, steeply northward-dipping planar structure of about 15–25 km thickness, extending in depth from about 40 to 240 km, with most seismicity concentrated in several clusters between 160 and 220 km depth. The geometry outlined by hypocenters reveals considerable structural complexity, being separated into an upper, rather planar and a lower, fragmented part by a seismic gap at about 150 km depth. The structurally simpler Pamir seismic zone defines an arc, which begins at the eastern end of the Hindu Kush seismic zone, where it strikes north-south and dips eastwards, then gradually bends around to reach an east-west strike and southward dip at its eastern termination. Earthquakes are confined to a narrow (10 km) curviplanar structure at depths of 80–150 km in the eastern part and 60–240 km in the western part of the arc. The dip angle is around 50° and constant along strike. The events extending deeper than 150 km in the west show a clear steepening of the structure to near-vertical. Seismicity in the Pamir is disconnected from shallow activity at the Main Pamir Thrust by an aseismic lower crust (25–70 km depth).

[35] We interpret the Pamir seismic zone as the consequence of southward descent of Eurasian continental lithosphere into the mantle. The thin planes outlined by seismicity most probably represent lower crustal material, possibly eclogitized, descending along with Eurasian mantle lithosphere. Both a classical subduction zone or the occurrence of sheet-like delamination could effect the observed geometry. The Hindu Kush seismic zone is most likely created by the same process, making its provenance likewise Eurasian. This would necessitate a process effecting the overturn of the Hindu Kush part of the structure. Evidence for such a process may be found in the complex geometry of the Hindu Kush with its seismicity clusters possibly representing plate fragments. However, a scenario in which continental India underthrusts Eurasia further south (MFT) and is forced to descend into the mantle at the locus of the Hindu Kush cannot be ruled out. The prevalence of thin planes again hints at the presence of continental crustal material at depth. The fragmentation of the lower Hindu Kush seismic zone could be the consequence of a complicated tearing and/or contortion process active here. The complete earthquake catalog analyzed herein is supplied as an electronic supplement to this article.

Appendix A: Automatized Phase Picking and Hypocentral Location

[36] The automatic procedure we implemented demonstrates a way to produce a complete catalog of well-located earthquakes and reliable arrival time picks for *P* and *S* phases together with their quality classification starting from a large continuous set of off-line passive seismic network data. While well-performing automatic triggers and targeted pickers for *P* and *S* phases have been available for some time [e.g., *Allen*, 1978; *Baer and Kradolfer*, 1987; *Cichowicz*, 1993; *Aldersons*, 2004; *Diehl*, 2008; *Küperkoch et al*., 2010] and are rapidly becoming more important due to the growing amount of globally recorded waveform data, retrieving a reliable earthquake catalog by their application is still not a standard procedure. Trigger algorithms produce interminable lists of possible phase onsets from which only a small minority can be associated to seismic events that can be located. Since targeted phase pickers depend on the correct placement of windows around the expected phase, for which either a good first detection or an accurate travel-time prediction (which depends on the event location) is needed (section A2), event association, location, and phase-picking are highly inter-dependent. This can only be overcome by iteratively improving a location and adding or improving phase picks based on the updated location in each step (sections A1–A4).

[37] It is the calibration of the processing chain, i.e., testing when a pick should be considered a mispick and defining when a location can be considered "good," that is the most work-intensive part of the implementation. It needs a carefully handpicked subset of events representative of the region's seismicity in order to calibrate parameters in the detection, association, and phase-picking and to

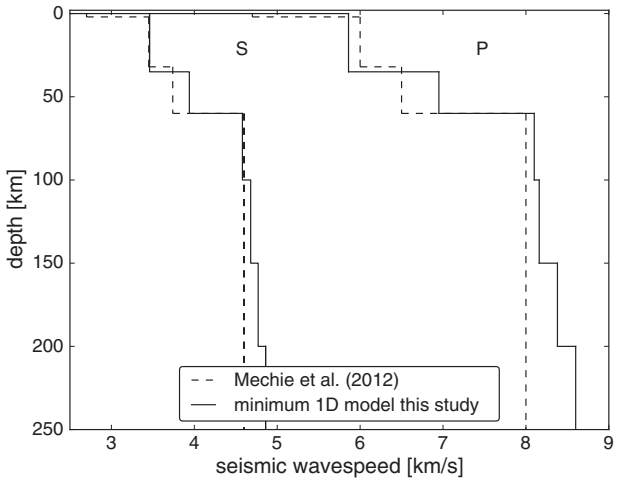

Figure A1. Comparison of velocity models of *Mechie et al.* [2012] (initial model before 2-D inversion; dashed lines) and the minimum 1-D model obtained in this study (solid lines).

critically validate the whole procedure's performance (section A5). We have demonstrated that the accuracy of the automatically determined phase picks is comparable to manual picking, which ensures high-quality locations and makes the picks also suitable for, e.g., tomographic inversion. We tuned the phase-pick weighting to be conservative, i.e., to eliminate/downweigh picks rather than keep blunders. However, this resulted in a relatively low hit-rate for phase-picks compared to manual analysis.

[38] In the following, the single processing steps applied in order to retrieve the hypocentral locations shown in the main part of the paper are described.

A1. Preliminary P Picks and Locations

[39] All vertical component waveform data were examined with a recursive STA/LTA trigger algorithm [as in *Withers et al.*, 1998] with an adaptive trigger threshold; i.e., the threshold was defined as the 99.9% quantile of the characteristic function. This ensures a roughly constant amount of alerts for each station and day, which was calibrated to capture all background seismicity. During seismicity swarms and aftershock series, this implementation leads to smaller events possibly being missed (depending on the activity level). Slightly more than $4*10^6$ trigger alerts were determined in this step, by far not all of them, however, related to actual earthquakes. The association of preliminary picks to preliminary events was performed using Binder (Rietbrock and Heath, personal communication, 2010), a program which uses a grid search approach on a rough orthorhombic grid of the region of interest, based on a preliminary 1-D velocity model [used by *Mechie et al.*, 2012, as starting model for 2-D inversion in the eastern Pamir]. Traveltimes from each station to each lattice node are calculated, subsequently a time window is propagated over the stack of trigger alert times, and consistent origin times at one node are searched for looking for consistent travel times on the grid. An event is declared if origin times at one node are produced from the trigger alert stack within a user-defined error margin. Thus, most false trigger alerts are sorted out, whereas earthquakes consistently appearing in the seismic records of several stations at the right time are retained. The obtained events were finally relocated using Geiger's [*Geiger*, 1910] least squares inversion method (i.e., HYPO71) [*Lee and Lahr*, 1975].

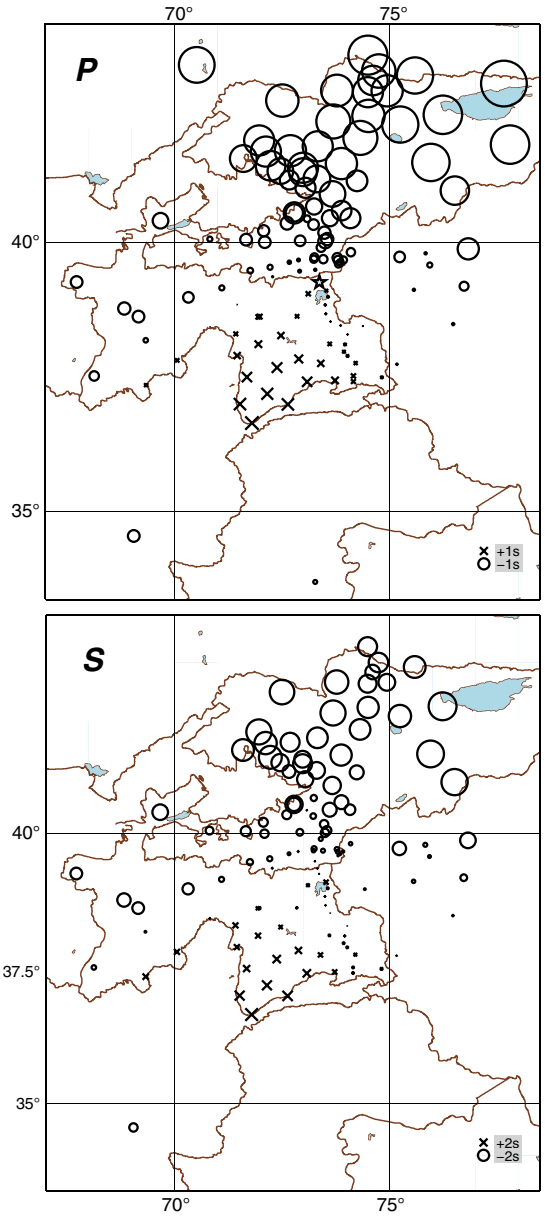

Figure A2. Static station corrections for *P* (above) and *S* (below) phases determined from a joint inversion for 1-D velocity model, hypocenters, and station corrections for a reference data set of 1780 automatically retrieved events consisting of 55,812 *P* and 30,699 *S* picks. Circles denote negative, plus signs positive station corrections. Starting model and final 1-D velocity model are shown in Figure A4. Only stations with at least 20 arrival times in the reference data set are shown. The reference station, constrained to have a *P* correction of zero, is shown with a star in the upper subfigure.

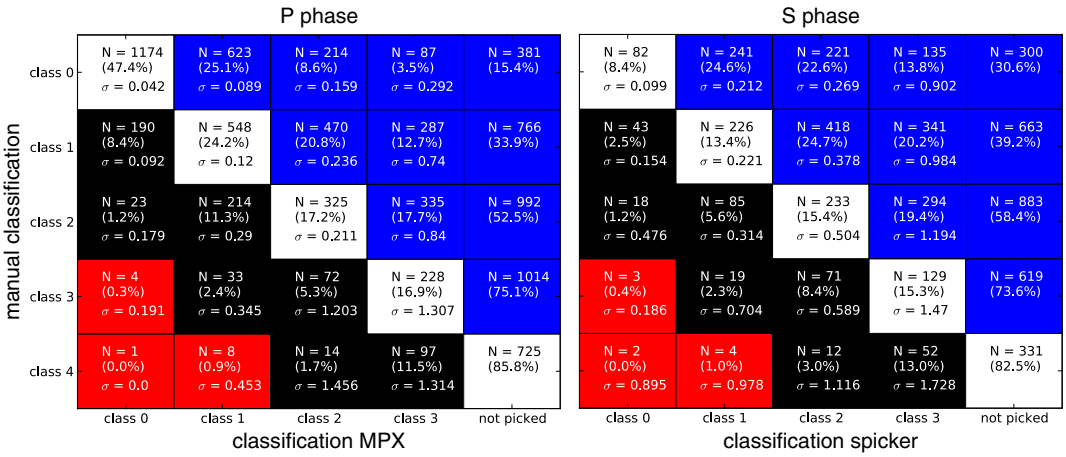

Figure A3. Confusion matrices for *P* (left) and *S* (right) picks, comparing handpicks to the ones obtained by the automatic procedure described in the text. A confusion matrix is a way of representing the performance of any kind of classification algorithm that is often used in machine learning [for definition, see *Kohavi and Provost*, 1998] and has been recently adopted for the evaluation of automatic seismic arrival time picking algorithms [e.g., *Di Stefano et al*., 2006; *Diehl et al*., 2009b; *Küperkoch et al*., 2010]. Its columns here refer to the weighting classes as assigned by the two picking algorithms (whose performance is to be evaluated), and its rows represent the weighting scheme applied by the human analyst (which is the reference here). The standard deviation of residuals between automatic and manual picks is given for each field (summed values for the columns are presented in Table A1). Percentages indicate the fraction of all manually determined arrivals of a certain quality class that are assigned a specific weight by the automatic procedure and sum up to 100% in each line of the confusion matrix. The conservative nature of quality weighting performed by the algorithms is discernible in the scarcity of picks falling into the black and red fields below the diagonal, which means that picks are rather downgraded than upgraded.

A2. Repicking of P

[40] Based on these preliminary locations and picks, *P* onsets were repicked with the MPX algorithm [*Aldersons*, 2004; *Di Stefano et al.*, 2006]. This code performs a three-step procedure, consisting of the application of a Wiener filter [*Douglas*, 1997], running the picker of *Baer and Kradolfer* [1987] on the filtered data, and a quality weighting procedure relying on Fisher statistics. With the Wiener filter, the constituent noise frequency bands are suppressed in the signal. This has the advantage of not changing the characteristics (and thus also potentially the onset times) of the signal as, e.g., a standard Butterworth bandpass filter would [*Douglas*, 1997], but it requires the input of two time windows, one in the noise and one in the signal, for spectral analysis to be applied in order to find these constituent frequencies of noise and signal. Hence, MPX can only be applied as a secondary picker, when a preliminary *P* pick around which these windows can be placed already exists [*Diehl et al*., 2009a, Figure 5].

[41] MPX was set up to classify onsets into four quality classes (0 to 3) [Table A1). The weighting scheme was calibrated with a hand-picked reference data set (section A5) following the procedure outlined in *Diehl and Kissling* [2008].

[42] To exclude effects caused by the different frequency responses of the various sensor types, all vertical waveform

Table A1. Uncertainties Associated With the Single Picking Quality Classes for *P* and *S* Onsets[a]

Quality Class	Handpicking Goal [s]	Handpicking Variance [s]	Variance Autopicker [s]	Points for Cumulative Sum
P_0	0.05	0.045	0.051	4
P_1	0.1	0.130	0.139	3
P_2	0.2	0.304	0.293	2
P_3	>0.2	0.669	0.914	1
S_0	0.1	0.162	0.173	8
S_1	0.2	0.712	0.252	6
S_2	0.4	0.775	0.408	4
S_3	>0.4	1.124	1.144	2

[a]Handpicking variance was defined as the average deviation between earliest and latest pick of four human analysts picking the same data set. Autopicking variance is the mean standard deviation of residuals between automatic pick and one (reference) human analyst (columns of the confusion matrices in Figure A3). The last column lists the contribution of each pick of a class to the cumulative sum used for event selection (see text).

data were converted to a Mark Products L4C seismometer response with 1 Hz eigenfrequency. For the local, mostly small to moderately sized earthquakes encountered here, this filter proved to be appropriate. In the next step, the STA/LTA arrival times were taken as the preliminary *P* estimate around which the time windows on the waveform data were placed. If a good pick (classes 0 or 1) was obtained with this configuration, it was accepted. In the other cases (classes 2 or 3), MPX was run multiple times with systematically varying window placements to account for the uncertainty in the preliminary onset estimates, and earlier and/or higher-quality arrivals were chosen to replace the initial pick.

[43] In the case of no arrival being found for an STA/LTA-derived preliminary *P* estimate, the vicinity (6 s before until 2 s after the estimate, in steps of 0.5 s; asymmetry due to the tendency of STA/LTA picks being late) of this STA/LTA arrival was examined iteratively, and the highest-quality arrival obtained in this way was accepted. When two or more arrivals of the same quality class were found, the earliest one was accepted. If no arrival was found, the station with its STA/LTA pick was discarded for this event.

[44] As the event association process with Binder (section A1) falsely discards a substantial amount of STA/LTA trigger alerts in the first step, stations with no STA/LTA pick were likewise iteratively examined with MPX. In this case, the first reference *P* estimate, around which the search window was defined, came from raytracing [NonLinLoc package, *Lomax et al.*, 2000] based on the preliminary event location and the preliminary 1-D velocity model. Since these locations are generally not very precise and the velocity model is not necessarily appropriate everywhere, the window in which the *P* arrival was searched for iteratively was doubled compared to the case where an STA/LTA pick existed.

[45] Based on the refined *P* picks obtained in this manner, all events were relocated using an iterative procedure based on multiple HYPO71 calls. For each event, a subset of picks

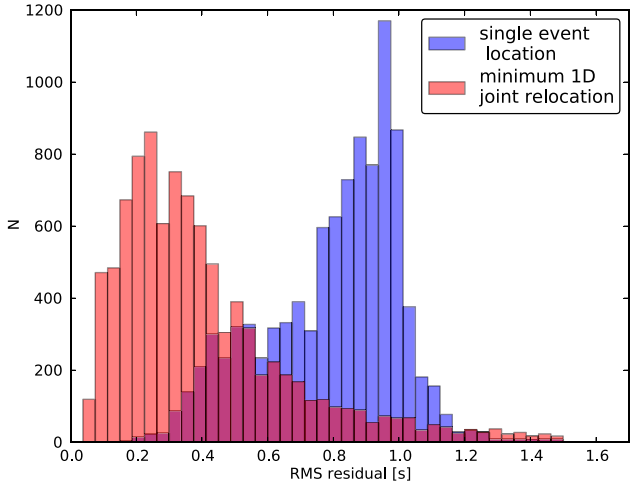

Figure A4. Histograms of RMS travel time residuals obtained for the relocation of events after the *S* picking step, using the velocity model of *Mechie et al.* [2012] and single event location (blue) and after relocation with the minimum 1-D model and station corrections (red).

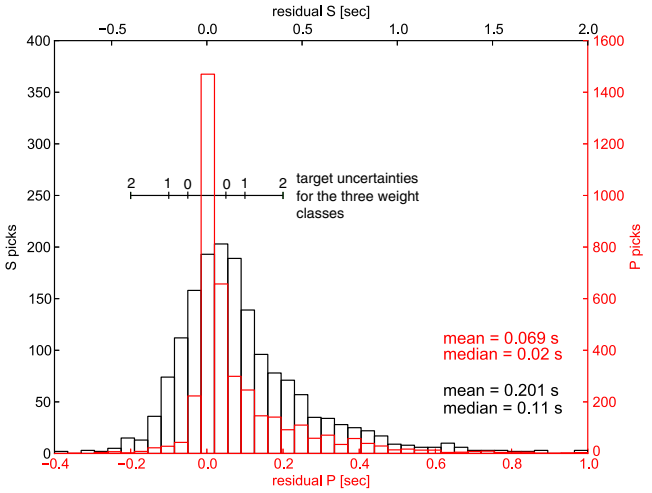

Figure A5. Histograms of residuals between handpicks and automatic picks for *P* and *S* onsets, classes 0–2. Negative time values refer to the automatic pick being earlier than the handpick. Formal picking errors for classes 0, 1, and 2 are indicated by error bars around zero. Note that the horizontal axis is enlarged by a factor of 2 for *S* residuals.

which had the best quality classes and the shortest travel times was selected, and a first location was performed for these picks only. This first location, based solely on reliable picks, serves as reference against which the more dubious picks (lower quality classes, greater distance from event) were subsequently tested. In case the root mean square (RMS) residual of this location was higher than 1 s, different starting depths were tried. If this did not yield a location with acceptable RMS residual, the pick with the highest single residual was removed. This was repeated until a good location was found. In a second step, the picks with lower quality estimates and those from more distant stations were incorporated. This was done one pick at a time, and a pick was only kept if after relocation the single residual of the new pick fell below a distance-dependent goal residual (0.6 s + (traveltime)*0.015). The rationale for performing this procedure is that a large amount of systematically shifted low-quality picks might, if added at the same time, dominate the location and thus effect a sorting out of the "better" (e.g., nearer and higher-quality) picks. All in all, 22,869 events, consisting of 380,626 *P* picks, were obtained in this step.

A3. S Picking

[46] Subsequently, *S* onsets were automatically determined using the software *spicker* [*Diehl et al.*, 2009b], which combines three different strategies of identifying *S* picks:

[47] 1. The *S*-phase picker of *Cichowicz* [1993], which declares the *S* onset where the product of three parameters, i.e., deflection angle, degree of polarization, and ratio of transverse to total energy, rises above a threshold.

[48] 2. An STA/LTA detector applied to the horizontal components.

[49] 3. An autoregressive Akaike Information Criterion (AR-AIC) based predictive picking algorithm as described in *Takanami and Kitagawa* [1988].

[50] With each of these single algorithms, an earliest and latest possible pick are determined, and the widths of these single "pick windows" as well as the consistency of the three methods yield quality classes of the picks. *spicker* hence requires a good P pick (needed for the polarization analysis and the choice of several time windows), an event location and a preliminary *S* pick.

[51] We applied *spicker* to our stack of relocated events with MPX-based *P* phases. The preliminary *S* arrivals were determined by raytracing. *spicker* was calibrated to rate picks into four quality classes as above (Table A1).

[52] After adding *S* arrivals, events were again relocated, using the same procedure as outlined for the P picks, only allowing for greater single residuals for the stations with low-quality arrivals and/or large hypocentral distances (cut-off value 1.0 s + (traveltime)*0.015). It should be mentioned that we allowed the possibility of further *P* picks being removed should they, and not the newly added *S* picks, have the greatest single residuals.

[53] After this step, our catalog contained 22,858 events with 370,013 *P* picks and 149,332 *S* picks. A selection procedure was applied subsequently in order to choose only the most robustly located earthquakes from our data set. A cumulative pick sum was calculated for each event in the following way: P picks of quality classes 0, 1, 2, or 3 add 4, 3, 2 ,or 1 point(s) to this sum, respectively. *S* picks count doubly compared to *P* picks (Table A1). Only events which had a cumulative sum above 50, with at least 16 points coming from S arrivals, were selected. This second constraint was necessary to exclude some regional events that were falsely located into our region of interest based only on P picks (no S picks were determined for those events because of grossly false window placement within *spicker*). This resulted in the set of 9532 well-located earthquakes comprising 197,951 *P* picks and 104,471 *S* picks that will be analyzed further below.

A4. Determination of Minimum 1-D Velocity Model and Relocation

[54] Following the procedure outlined in *Kissling et al.* [1994], we simultaneously inverted for a minimum 1D velocity model, hypocentral parameters and static station corrections using the program VELEST. A declustered reference data set consisting of 1780 events, comprising 55,812 *P* and 30,699 *S* picks, was selected by subdividing the study area into subregions and selecting only the best located events respectively. The 1D velocity model of *Mechie et al.* [2012] (their starting model for 2D inversion) was used as the initial model. A Wadati diagram for all available events yielded an average vp/vs ratio of approximately 1.74, which was used for the initial S model in the inversion procedure.

[55] Due to the substantial extent and extreme geological heterogeneity of the study area, the retrieved 1-D model (Figure A4) is rather crude and only represents a large-scale average over the study region. A shallow sediment layer, present in the model of *Mechie et al.* [2012] derived for the eastern Pamir, could not be resolved. Thus, most of the travel time differences caused by heterogeneity in the crust and mantle throughout the region of interest were mapped into the station corrections (Figure A5). A trend from massively negative station corrections in northern Kyrgyzstan and around the Ferghana Valley and (to a lesser degree) in most parts of the Tajik Depression to positive values in and around the Pamir is discernible. Since seismicity in our dataset is mainly concentrated in the southern and central part of the network, stations in the north have longer average path lengths and hence may accumulate large absolute travel time residuals due to deviations of the real Earth from the 1D model, which leads to large station corrections.

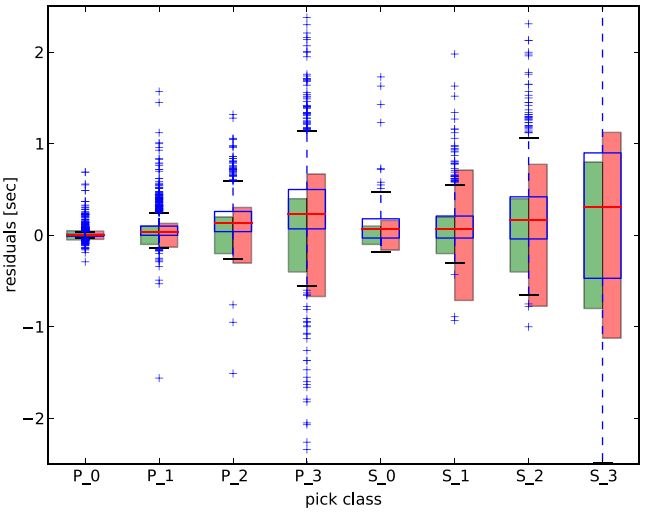

Figure A6. Boxplot of the distributions of residuals between automatically and manually determined picks for *P* and *S* arrivals of a reference data set of 230 events, sorted by quality class. The red horizontal line in each boxplot is the median value, and the blue box around it defines the inner quartile range, i.e., 50% of the data are within this box. The whiskers (dashed blue lines) extend to the furthest data point within another 1.5 times this inner quartile range, and points outside this range are plotted as blue plus signs. Superimposed on this are the goal uncertainties for each quality class as listed in Table A1 (green bars) and the actual variability in handpicked arrival times obtained by four human analysts (red bars).

[56] All events in the catalog were re-located using the VELEST-derived 1-D velocity model and station phase terms. Picks with residuals more than two standard deviations from the event's mean residual and with an absolute value above 1 s were sorted out, which led to a total reduction of 2.49% in *P* picks and 6.17% in *S* picks. Figure A6 shows the improvement in RMS residuals between locations using the preliminary velocity model and the minimum 1D model with station corrections. Obtained relocations not only show lower RMS residuals, but likewise define sharper structures compared to the preliminary ones, as illustrated in Figures 3a and 3b.

A5. Quality Assessment

[57] In order to assess the performance of the whole automated picking and location procedure, a reference data set consisting of 230 events was carefully handpicked (8825 *P* and 5538 *S* picks), guided by the weighting scheme shown in Table A1.

[58] The picking and weighting performance of the whole automated procedure is compared to the human analysts'

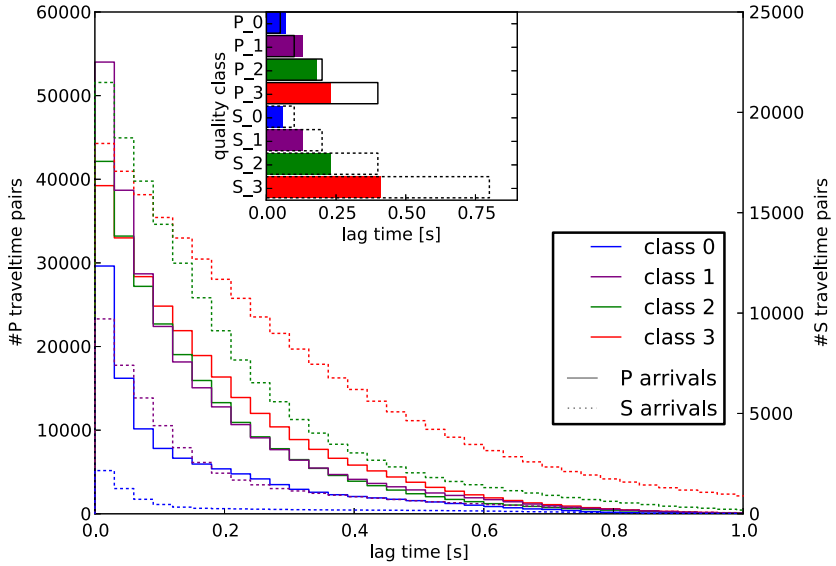

Figure A7. Cumulative histogram of CC lag times, shown for all *P* and *S* quality classes. For each event pair at one station, the lower of the two picking quality classes was chosen to define overall quality. Differences between the quality classes are discernible, a greater proportion of small lags is observed for the higher quality classes. In the inset, the 68% quantile of the lag times for each quality class, taken as a proxy for standard deviation (which can not be determined for a one-sided distribution), shown as colored bars, is compared to the formal picking errors (black bar frames) defined in Table A1. Obtained lag values for *P* correspond well to formal errors; for *S*, they are even substantially smaller.

picks in two confusion matrices (Figure A3). The hit rates we obtain are relatively low (56.4% of the human analyst for P, 49.9% for S), which is not only due to the rather conservative nature of the two picking algorithms' weighting schemes [see *Di Stefano et al*., 2006; *Diehl et al*., 2009b], but also reflects the loss of some picks in the multiple relocations along our processing chain. Our automated classification is shown to be conservative, as we observe nearly no picks being upgraded from the lowest visually assigned quality classes to the highest automatic ones (red fields in the confusion matrices).

[59] In order to evaluate the real uncertainties behind the automatically assigned weighting classes we obtained for our data set, we have to evaluate the columns of the confusion matrices. Except for the lowest automatic class 3, the summed standard deviations of residuals are near the goal uncertainties for handpicking (Table A1), and residuals are systematically smaller for higher quality classes. Histograms for residuals between handpicks and automatic picks, summed for quality classes 0 to 2 (i.e., the three leftmost columns in the confusion matrices in Figure A3), are shown in Figure A1.

[60] Since the uncertainties listed in Table A1 are only goals, the implementation of which by human observers may substantially differ, we performed a test comparing four different analysts handpicking the same subset of the reference data set.

[61] A comparison of the automated procedure's accuracy for each quality class is shown as a boxplot in Figure A2. The distribution of residuals (i.e., pick time difference human analyst—automatic pick) is shown for each (automatic) quality class for *P* and *S*. Superimposed are the goal uncertainties (green bars) and the mean pick variability between the four human analysts. For the determination of this last quantity, each trace that was picked by at least two of the four analysts was evaluated, an average weighting class was determined (rounded mean of the assigned classes), and the absolute time difference between earliest and latest handpick was calculated. The means of all these differences, for each average weighting class, are displayed as red bars in Figure A2. It is evident that when picking S onsets, the human analysts do not reach the uncertainty goals of the quality classes.

[62] Figure A2 and Table A1 show that, with the exception of the classes P_3 and S_3, the automatically obtained picks do not substantially deviate from what a human analyst would determine. In the case of S picks, the humans' performance may even be inferior to that of the algorithm. The retrieved quality classes scale with uncertainty (here taken as residual human-autopicker), and these uncertainties are not much higher (*P*) or even substantially lower (*S*) than the mean variance between different human analysts. The main caveats of the automatic procedure are the lower hit rate compared to handpicking and a slight tendency of automatic picks being later than manually determined ones (Figure A1).

[63] A final quality estimate for obtained picks that does not rely on any human reference analyst comes from the application of waveform cross-correlation (section A7). Pairs of arrival times for clustered events at a single station were utilized and the optimum time lag; i.e., the amount of time one trace has to be shifted relative to the other in order to optimally align them, was determined. Results of this procedure are shown in Figure A7. We observe that the lag times scale with quality class (larger lags for lower classes) and that the standard deviation of lags is comparable to (for *P* arrivals) or smaller than (for *S* arrivals) formal picking errors for each class.

A6. Magnitudes

[64] Local magnitudes (M_L) were calculated for all earthquakes using the approach of *Hutton and Boore* [1987]. An alternative set of coefficients, distinguishing between shallow and deep seismicity in the calculation of the respective values of M_L [*Shin*, 1993] yielded comparable magnitudes. The distribution of magnitudes among all events is shown in Figure 5 (lower right). From the histogram, a magnitude of completeness of around 2.5 can be deduced. However, this value should vary substantially with region and time due to our heterogeneous and changing network geometry.

A7. Double-difference Relocations

[65] To further refine the hypocenter locations, our catalog of earthquakes was relocated once more using a double-difference (DD) scheme (HypoDD) [*Waldhauser and Ellsworth*, 2000]. The DD method relates travel time differences of pairs of events to the same station to their spatial separations and therefore cancels out the correlated errors arising from unmodeled structure along the segment of the path they share. It has been shown to be particularly effective if precise differential travel times from waveform cross-correlation are used. Cross correlation (CC) based travel time differences are often an order of magnitude more precise than the ones derived from phase picks. A further advantage of using CC travel time differences is that measurements are done algorithmically, not relying on analyst intervention, making it particularly suitable for large data sets. We calculated CC based differential travel times (for *P* and *S*) both for events with and without phase picks. In the latter case we used ray tracing to place the CC windows. In this way we replenish our data set with phase measurements that may have been missed due to our limited hit-rate in arrival time picking. Cross correlation measurements were done for events separated by not more than 15 km with windows of 2/4 s for *P*/*S* phases in the case that arrival time picks existed and longer 4/6 s windows in the case that theoretical arrival times were used, in order to compensate for the larger uncertainty in the window placements. Only measurements with a correlation coefficient >0.7 [see tests in *von Seggern*, 2009] were kept, with the correlation coefficient used as a weight in the hypocenter inversion.

[66] Totally, 8207 earthquakes were relocated with hypoDD, utilizing 180,096 P and 130,134 S cross-correlation phase pairs as well as 1,013,650 *P* and 480,864 *S* differential arrival times from the catalog. A weighting scheme was implemented that starts the inversion exclusively with the catalog phase pairs, then successively down-weighs those and assigns higher weights to the cross-correlation phase pairs. The overall RMS residual was reduced from 0.239 to 0.184 s (–23.0%) for the catalog arrivals and from 0.332 to 0.026 s (–92.2%) for the cross-correlation phase pairs in the course of the relocation.

[67] DD can only relocate events that have strongly linked measurements, i.e., that belong to spatial clusters. Hence, for events that could not be relocated by DD (e.g., because they are spatially isolated), we kept the locations derived in section A4. The improvement in hypocenter locations through the different steps of our relocation scheme is impressively demonstrated in an exemplary cross section in Figure 3. In this cross section, structures are clearly sharpened and hypocenters at mantle depths collapse to a plane less than 10 km thick, first steeply dipping east and then dropping vertically down to a sharp cut-off at approximately 250 km depth. This further sharpening of imaged structures indicates that our final location uncertainties should, for the DD relocations, be smaller than the estimates shown in Figure 4.

[68] **Acknowledgments.** The Python software package Obspy [http://obspy.org, *Beyreuther et al*., 2010] was used for various processing and data handling purposes. GMT [*Wessel and Smith*, 1998] was used for the compilation of several figures. Seismic waveform data was provided by IRIS (networks KN, KR, KZ, II, IU), GEOFON and the Xinjiang Seismological Bureau. The Geophysical Instrument Pool Potsdam (GIPP) provided the utilizied seismic stations. We likewise wish to express our gratitude to all field teams and drivers of projects TIPAGE and FERGHANA as well as the German Earthquake TaskForce, who contributed to the success of network installations in highly difficult terrain. C. Krumbiegel, M. Wieprich and C. Feld helped with seismic arrival time picking. This work was supported by Deutsche Forschungsgemeinschaft. Comments by Gary Pavlis and an anonymous reviewer helped to improve the manuscript.

References

Aldersons, F. (2004), Toward a three-dimensional crustal structure of the dead sea region from local earthquake tomography, Ph.D. thesis, Tel-Aviv University, Israel.

Allen, R. (1978), Automatic earthquake recognition and timing from single traces, *Bull. Seismol. Soc. Am.*, *68*(5), 1521–1532.

Arrowsmith, J. R., and M. Strecker (1999), Seismotectonic range-front segmentation and mountain-belt growth in the Pamir-Alai region, Kyrgyzstan (India-Eurasia collision zone), *Geol. Soc. Am. Bull.*, *111* (11), 1665–1683, doi:10.1130/0016-7606(1999)111<1665:SRFSAM>2.3.CO;2.

Avouac, J., and P. Tapponnier (1993), Kinematic model of active deformation in central Asia, *Geophys. Res. Lett.*, *20*(10), 895–898.

Baer, M., and U. Kradolfer (1987), An automatic phase picker for local and teleseismic events, *Bull. Seismol. Soc. Am.*, *77*(4), 1437–1445.

Bajolet, F., J. Galeano, F. Funiciello, M. Moroni, A. Negredo, and C. Faccenna (2012), Continental delamination: Insights from laboratory models, *Geochem. Geophys. Geosyst.*, *13* (1), 1–22, doi:10.1029/2011GC003896.

Bernard, M., B. Shen-Tu, W. Holt, and D. M. Davis (2000), Kinematics of active deformation in the Sulaiman Lobe and Range, Pakistan, *J. Geophys. Res.*, *105*, 13,253–13,279.

Beyreuther, M., R. Barsch, L. Krischer, T. Megies, Y. Behr, and J. Wassermann (2010), ObsPy: A Python toolbox for seismology, *Seismol. Res. Lett.*, *81*(3), 530–533, doi:10.1785/gssrl.81.3.530.

Billington, S., B. Isacks, and M. Barazangi (1977), Spatial distribution and focal mechanisms of mantle earthquakes in the Hindu Kush-Pamir region: A contorted Benioff zone, *Geology*, *5*(11), 699–704.

Bird, P. (1979), Continental delamination and the Colorado Plateau, *J. Geophys. Res.*, *84*(B13), 7561–7571.

Burov, E., and P. Yamato (2008), Continental plate collision, PTtz conditions and unstable vs. stable plate dynamics: Insights from thermo-mechanical modelling, *Lithos*, *103*(1-2), 178–204, doi:10.1016/j.lithos.2007.09.014.

Burtman, V., and P. Molnar, (1993), Geological and geophysical evidence for deep subduction of continental crust beneath the Pamir, *Geological Society of America Special Paper 281*, 76 pp., Boulder, Colo.

Chatelain, J., S. Roecker, D. Hatzfeld, and P. Molnar (1980), Microearthquake seismicity and fault plane solutions in the Hindu Kush region and their tectonic implications, *J. Geophys. Res.*, *85*(B3), 1365–1387.

Chemenda, A., J. Burg, and M. Mattauer (2000), Evolutionary model of the Himalaya-Tibet system: geopoem based on new modelling, geological and geophysical data, *Earth Planet. Sci. Lett.*, *174*(3-4), 397–409.

Cichowicz, A. (1993), An automatic S-phase picker, *Bull. Seismol. Soc. Am.*, *83*(1), 180–189.

Coutand, I., M. Strecker, J. R. Arrowsmith, G. Hilley, R. Thiede, A. Korjenkov, and M. Omuraliev (2002), Late Cenozoic tectonic development of the intramontane Alai Valley, (Pamir-Tien Shan region, central Asia): An example of intracontinental deformationdue to the Indo-Eurasia collision, *Tectonics*, *21*(6), 1053, doi:10.1029/2002TC001358.

Coward, M., and R. Butler (1985), Thrust tectonics and the deep structure of the Pakistan Himalaya, *Geology*, *13*, 417–420.

Cowgill, E. (2010), Cenozoic right-slip faulting along the eastern margin of the Pamir salient, northwestern China, *Geol. Soc. Am. Bull.*, *122*(1-2), 145–161, doi:10.1130/B26520.1.

DeCelles, P. G., D. Robinson, and G. Zandt (2002), Implications of shortening in the Himalayan fold-thrust belt for uplift of the Tibetan Plateau, *Tectonics*, *21*(6), 1–25, doi:10.1029/2001TC001322.

DeMets, C., R. G. Gordon, and D. F. Argus (2010), Geologically current plate motions, *Geophys. J. Int.*, *181*(1), 1–80, doi:10.1111/j.1365-246X.2009.04491.X.

Di Stefano, R., F. Aldersons, E. Kissling, P. Baccheschi, C. Chiarabba, and D. Giardini (2006), Automatic seismic phase picking and consistent observation error assessment: Application to the Italian seismicity, *Geophys. J. Int.*, *165*(1), 121–134, doi:10.1111/j.1365-246X.2005.02799.X.

Diehl, T. (2008), 3-D seismic velocity models of the Alpine crust from local earthquake tomography, Ph.D. thesis, ETH Zürich.

Diehl, T., and E. Kissling (2008), Users guide for MPX picking system; Appendix D of T. Diehl's, Ph.D. thesis, ETH Zürich.

Diehl, T., E. Kissling, S. Husen, and F. Aldersons (2009a), Consistent phase picking for regional tomography models: Application to the greater Alpine region, *Geophys. J. Int.*, *176*(2), 542–554, doi:10.1111/j.1365-246X.2008.03985.X.

Diehl, T., N. Deichmann, E. Kissling, and S. Husen (2009b), Automatic S-wave picker for local earthquake tomography, *Bull. Seismol. Soc. Am.*, *99*(3), 1906–1920, doi:10.1785/0120080019.

Douglas, A. (1997), Bandpass filtering to reduce noise on seismograms: Is there a better way?, *Bull. Seismol. Soc. Am.*, *87*(4), 770–777.

Ducea, M., et al. (2003), Building the Pamirs: The view from the underside, *Geology*, *31*(10), 849, doi:10.1130/G19707.1.

Eneva, M., M. Hamburger, and G. Popandopulo (1992), Spatial distribution of earthquakes in aftershock zones of the Garm region, Soviet Central Asia, *Geophys. J. Int.*, *109*(1), 38–53, doi: 10.1111/j.1365-246X.1992.tb00077.X.

Fan, G., J. Ni, and T. Wallace (1994), Active tectonics of the Pamirs and Karakorum, *J. Geophys. Res.*, *99*(B4), 7131–7160.

Geiger, L. (1910), Herdbestimmung bei Erdbeben aus den Ankunftszeiten, *K. Gesellschaft d. Wiss. Göttingen*, *4*, 331–349.

Gögüs, O. H., and R. N. Pysklywec (2008), Near-surface diagnostics of dripping or delaminating lithosphere, *J. Geophys. Res.*, *113*(B11), 1–11, doi:10.1029/2007JB005123.

Gordon, S. M., P. Luffi, B. Hacker, J. Valley, M. Spicuzza, R. Kozdon, P. Kelemen, L. Ratschbacher, and V. Minaev (2012), The thermal structure of continental crust in active orogens: Insight from Miocene eclogite and granulite xenoliths of the Pamir Mountains, *J. Metamorph. Geol.*, *30*(4), 413–434, doi:10.1111/j.1525-1314.2012.00973.X.

Govers, R., and M. Wortel (2005), Lithosphere tearing at STEP faults: Response to edges of subduction zones, *Earth Planet. Sci. Lett.*, *236* (1-2), 505–523, doi:10.1016/j.epsl.2005.03.022.

Gray, R., and R. N. Pysklywec (2012), Geodynamic models of mature continental collision: Evolution of an orogen from lithospheric subduction to continental retreat/delamination, *J. Geophys. Res.*, *117*(B3), 1–14, doi: 10.1029/2011JB008692.

Guillot, S. (2003), Reconstructing the total shortening history of the NW Himalaya, *Geochem. Geophys. Geosyst.*, *4*(7), 1064, doi:10.1029/2002GC000484.

Gutenberg, B., and C. Richter (1954), *Seismicity of the Earth and Associated Phenomena*, Prinecton University Press, Princeton, NJ.

Haberland, C., U. Abdybachaev, B. Schurr, H.-U. Wetzel, S. Roessner, A. Sarnagoev, S. Orunbaev, and C. Janssen (2011), Landslides in southern Kyrgyzstan: Understanding tectonic controls, *Eos Trans. AGU*, *92*(20), 169–170, doi:10.1007/s11069-.

Hacker, B. (2003), Subduction factory 1. Theoretical mineralogy, densities, seismic wave speeds, and H 2 O contents, *J. Geophys. Res.*, *108*(B1), 1–26, doi:10.1029/2001JB001127.

Hacker, B. (2005), Near-ultrahigh pressure processing of continental crust: Miocene crustal xenoliths from the Pamir, *J. Petrol.*, *46*(8), 1661–1687, doi:10.1093/petrology/egi030.

Hacker, B., S. Peacock, G. Abers, and S. G. Holloway (2003), Subduction factory 2. Are intermediate-depth earthquakes in subducting slabs linked to metamorphic dehydration reactions?, *J. Geophys. Res.*, *108*(B1), 549–553, doi:10.1029/2001JB001129.

Haq, S. S. B., and D. M. Davis (1997), Oblique convergence and the lobate mountain belts of western Pakistan, *Geology*, *25*(1), 23–26, doi: 10.1130/0091-7613(1997)025<0023:OCATLM>2.3.CO;2.

Hetényi, G., R. Cattin, F. Brunet, L. Bollinger, J. Vergne, J. Nábelek, and M. Diament (2007), Density distribution of the India plate beneath the Tibetan plateau : Geophysical and petrological constraints on the kinetics of lower-crustal eclogitization, *Earth Planet. Sci. Lett.*, *264*, 226–244, doi:10.1016/j.epsl.2007.09.036.

Houseman, G., D. McKenzie, and P. Molnar (1981), Convective instability of a thickened boundary layer and its relevance for the thermal evolution of continental convergent belts, *J. Geophys. Res.*, *86* (B7), 6115–6132.

Hutton, L., and D. Boore (1987), The ML scale in southern California, *Bull. Seismol. Soc. Am.*, *77*(6), 2074–2094.

Ismail-Zadeh, A., L. Matenco, M. Radulian, S. Cloetingh, and G. F. Panza (2012), Geodynamics and intermediate-depth seismicity in Vrancea (the south-eastern Carpathians): Current state-of-the art, *Tectonophysics*, *530-531*, 50–79, doi:10.1016/j.tecto.2012.01.016.

John, T., S. Medvedev, L. H. Rüpke, T. B. Andersen, Y. Y. Podladchikov, and H. Austrheim (2009), Generation of intermediate-depth earthquakes by self-localizing thermal runaway, *Nat. Geosci.*, *2*(2), 137–140, doi: 10.1038/ngeo419.

Jung, H., H. Green, and L. F. Dobrzhinetskaya (2004), Intermediate-depth earthquake faulting by dehydration embrittlement with negative volume change, *Nature*, *428*, 545–549, doi:10.1038/nature02412.

Kelemen, P., and G. Hirth (2007), A periodic shear-heating mechanism for intermediate-depth earthquakes in the mantle, *Nature*, *446*, 787–790, doi: 10.1038/nature05717.

Kind, R., and X. Yuan (2010), Seismic images of the biggest crash on Earth, *Science*, *329*(5998), 1479–1480, doi:10.1126/science.1191620.

Kind, R., et al. (2002), Seismic images of crust and upper mantle beneath Tibet: Evidence for Eurasian plate subduction, *Science*, *298*, 1219–1221, doi:10.1126/science.1078115.

Kirby, S., S. Stein, E. Okal, and D. Rubie (1996), Metastable mantle phase transformations and deep earthquakes in subducting oceanic lithosphere, *Rev. Geophys.*, *34*(2), 261–306.

Kissling, E., W. Ellsworth, D. Eberhart-Phillips, and U. Kradolfer (1994), Initial reference models in local earthquake tomography, *J. Geophys. Res.*, *99*(B10), 19,635–19,646.

Kohavi, R., and F. Provost (1998), Glossary of terms, *Machine Learning*, *30*(2/3), 271–274.

Konopaltsev, I. (1970), Study of movement of the earth's crust in the experimental polyon near Garm, *Izvestiya Acad. Sci. UdSSR Earth Phys. (in Russian)*, *6*, 71–76.

Kosarev, G., R. Kind, S. V. Sobolev, X. Yuan, W. Hanka, and S. Oreshin (1999), Seismic evidence for a detached Indian lithospheric mantle beneath Tibet, *Science*, *283*, 1306–1309, doi: 10.1126/science.283.5406.1306.

Koulakov, I. (2011), High-frequency P and S velocity anomalies in the upper mantle beneath Asia from inversion of worldwide traveltime data, *J. Geophys. Res.*, *116*(B4), 1–22, doi:10.1029/2010JB007938.

Koulakov, I., and S. V. Sobolev (2006), A tomographic image of Indian lithosphere break-off beneath the Pamir-Hindukush region, *Geophys. J. Int.*, *164*(2), 425–440, doi:10.1111/j.1365-246X.2005.02841.X.

Küperkoch, L., T. Meier, J. Lee, W. Friederich, and E. Working Group (2010), Automated determination of P -phase arrival times at regional and local distances using higher order statistics, *Geophys. J. Int.*, *181*, 1159–1170, doi:10.1111/j.1365-246X.2010.04570.X.

Lee, W., and J. Lahr (1975), Hypo71 (revised): A computer program for determining hypocenter, magnitude, and first motion pattern of local earthquakes, *US Geol. Surv. Open File Report*, *75-311*, 1–113.

Leech, M. (2001), Arrested orogenic development: Eclogitization, delamination, and tectonic collapse, *Earth Planet. Sci. Lett.*, *185*, 149–159.

Levander, A., B. Schmandt, M. S. Miller, K. Liu, K. E. Karlstrom, R. S. Crow, C.-T. A. Lee, and E. D. Humphreys (2011), Continuing Colorado plateau uplift by delamination-style convective lithospheric downwelling, *Nature*, *472*, 461–465, doi:10.1038/nature10001.

Li, C., R. van der Hilst, A. Meltzer, and E. Engdahl (2008), Subduction of the Indian lithosphere beneath the Tibetan Plateau and Burma, *Earth Planet. Sci. Lett.*, *274*(1-2), 157–168, doi:10.1016/j.epsl.2008.07.016.

Lister, G., B. Kennett, S. Richards, and M. Forster (2008), Boudinage of a stretching slablet implicated in earthquakes beneath the Hindu Kush, *Nat. Geosci.*, *1*(3), 196–201, doi:10.1038/ngeo132.

Lomax, A., J. Virieux, P. Volant, and C. Berge (2000), Probabilistic earthquake location in 3D and layered models: Introduction of a Metropolis-Gibbs method and comparison with linear locations, in *Advances in Seismic Event Location*, edited by Thurber, C., and N. Rabinowitz, Kluwer, Amsterdam, pp. 101–134.

Lorinczi, P., and G. Houseman (2009), Lithospheric gravitational instability beneath the Southeast Carpathians, *Tectonophysics*, *474*(1-2), 322–336, doi:10.1016/j.tecto.2008.05.024.

Maheo, G., S. Guillot, J. Blichert-Toft, Y. Rolland, and A. Pecher (2002), A slab breakoff model for the Neogene thermal evolution of South Karakorum and South Tibet, *Earth Planet. Sci. Lett.*, *195*(1-2), 45–58, doi: 10.1016/S0012-821X(01)00578-7.

Martynov, V., P. Molnar, T. Rautian, and V. Khalturin (1976), Preliminary results of an investigation of spectra of earthquakes in the Garm region in light of problems of the prediction of strong earthquakes, in *Sbornik of Soviet-American Work on the Prediction of Earthquakes, vol. 1 (in Russian)*, pp. 96–139.

Mechie, J., et al. (2012), Crustal and uppermost mantle velocity structure along a profile across the Pamir and southern Tien Shan as derived from project TIPAGE wide-angle seismic data, *Geophys. J. Int.*, *188*, 385–407, doi:10.1111/j.1365-246X.2011.05278.X.

Mohadjer, S., et al. (2010), Partitioning of India-Eurasia convergence in the Pamir-Hindu Kush from GPS measurements, *Geophys. Res. Lett.*, *37*(4), 1–6, doi:10.1029/2009GL041737.

Molnar, P., and D. Gray (1979), Subduction of continental lithosphere: Some constraints and uncertainties, *Geology*, *7*(1), 58–62.

Molnar, P., and J. M. Stock (2009), Slowing of India's convergence with Eurasia since 20 Ma and its implications for Tibetan mantle dynamics, *Tectonics*, *28*(3), 1–11, doi:10.1029/2008TC002271.

Molnar, P., and P. Tapponnier (1975), Cenozoic tectonics of Asia: Effects of a continental collision, *Science*, *189*(4201), 419–426.

Nábelek, J., G. Hetényi, J. Vergne, S. Sapkota, B. Kafle, M. Jiang, H. Su, J. Chen, B.-S. Huang, and HiClimb-Team (2009), Underplating in the Himalaya-Tibet collision zone revealed by the Hi-CLIMB experiment, *Science*, *325*, 1371–1374, doi:10.1126/science.1167719.

Negredo, A., A. Replumaz, A. Villaseñor, and S. Guillot (2007), Modeling the evolution of continental subduction processes in the Pamir-Hindu Kush region, *Earth Planet. Sci. Lett.*, *259* (1-2), 212–225, doi: 10.1016/j.epsl.2007.04.043.

Nersesov, I., and A. Semenov (1969), Seismic regionalization of the Garm region from the ratio of velocities of body waves, in *Seismic Regime*, Donish Publishers, Dushanbe, pp. 137–152.

Patriat, P., and J. Achache (1984), India-Eurasia collision chronology has implications for crustal shortening and driving mechanism of plates, *Nature*, *311*, 615–621.

Pavlis, G., and S. Das (2000), The Pamir-Hindu Kush seismic zone as a strain marker for flow in the upper mantle, *Tectonics*, *19*(1), 103–115.

Pegler, G., and S. Das (1998), An enhanced image of the Pamir-Hindu Kush seismic zone from relocated earthquake hypocentres, *Geophys. J. Int.*, *134*(2), 573–595, doi:10.1046/j.1365-246x.1998.00582.X.

Reigber, C., G. Michel, R. Galas, D. Angermann, J. Klotz, J. Chen, A. Papschev, R. Arslanov, V. Tzurkov, and M. Ishanov (2001), New space geodetic constraints on the distribution of deformation in Central Asia, *Earth Planet. Sci. Lett.*, *191* (1-2), 157–165, doi:10.1016/S0012-821X(01)00414-9.

Robinson, A. (2009), Geologic offsets across the northern Karakorum fault: Implications for its role and terrane correlations in the western Himalayan-Tibetan orogen, *Earth Planet. Sci. Lett.*, *279*(1-2), 123–130, doi:10.1016/j.epsl.2008.12.039.

Robinson, A., A. Yin, C. Manning, T. M. Harrison, S.-H. Zhang, and X.-F. Wang (2004), Tectonic evolution of the northeastern Pamir: Constraints from the northern portion of the Cenozoic Kongur Shan extensional system, western China, *Geol. Soc. Am. Bull.*, *116* (7), 953, doi: 10.1130/B25375.1.

Roecker, S. (1982), Velocity structure of the Pamir-Hindu Kush region: Possible evidence of subducted crust, *J. Geophys. Res.*, *87* (B2), 945–959.

Rudnick, R. (1995), Making continental crust, *Nature*, *378*, 571–578.

Rudnick, R., and D. M. Fountain (1995), Nature and composition of the continental crust: A lower crustal perspective, *Rev. Geophys.*, *33* (3), 267–309.

Schurr, B., A. Rietbrock, G. Asch, R. Kind, and O. Oncken (2006), Evidence for lithospheric detachment in the central Andes from local earthquake tomography, *Tectonophysics*, *415* (1-4), 203–223, doi: 10.1016/j.tecto.2005.12.007.

Schwab, M., et al. (2004), Assembly of the Pamirs: Age and origin of magmatic belts from the southern Tien Shan to the southern Pamirs and their relation to Tibet, *Tectonics*, *23*(4), TC4002, doi:10.1029/2003TC001583.

Searle, M. P. (1996), Geological evidence against large-scale pre-Holocene offsets along the Karakoram Fault: Implications for the limited extrusion of the Tibetan plateau, *Tectonics*, *15* (1), 171–186, doi: 10.1029/95TC01693.

Shin, T.-C. (1993), The calculation of local magnitude from the simulated Wood-Anderson seismograms of the short-period seismograms in the Taiwan area, *Terr. Atmos. Ocean Sci.*, *4*(2), 155–170.

Sobel, E., and T. Dumitru (1997), Thrusting and exhumation around the margins of the western Tarim basin during the India-Asia collision, *J. Geophys. Res.*, *102*(B3), 5043–5063, doi:10.1029/96JB03267.

Sobel, E., L. Schoenbohm, J. Chen, R. Thiede, D. Stockli, M. Sudo, and M. Strecker (2011), Late Miocene-Pliocene deceleration of dextral slip between Pamir and Tarim: Implications for Pamir orogenesis, *Earth Planet. Sci. Lett.*, *304*(3-4), 369–378, doi:10.1016/j.epsl.2011.02.012.

Sobel, E., J. Chen, L. Schoenbohm, R. Thiede, D. Stockli, M. Sudo, and M. Strecker (2013), Oceanic-style subduction controls late Cenozoic deformation of the Northern Pamir orogen, *Earth Planet. Sci. Lett.*, *363*, 204–218, doi:10.1016/j.epsl.2012.12.009.

Spakman, W., and R. Hall (2010), Surface deformation and slab-mantle interaction during Banda arc subduction rollback, *Nat. Geosci.*, *3* (8), 562–566, doi:10.1038/ngeo917.

Takanami, T., and G. Kitagawa (1988), A new efficient procedure for the estimation of onset times of seismic waves, *J. Phys. Earth*, *36* (6), 267–290.

Tapponnier, P., and P. Molnar (1979), Active faulting and Cenozoic tectonics of the Tien Shan, Mongolia, and Baykal regions, *J. Geophys. Res.*, *84*(B7), 3425–3459.

Tapponnier, P., M. Mattauer, F. Proust, and C. Cassaigneau (1981), Mesozoic ophiolites, sutures, and large-scale tectonic movements in Afghanistan, *Earth Planet. Sci. Lett.*, *52*(2), 355–371.

Tapponnier, P., G. Peltzer, A. L. Dain, R. Armijo, and P. Cobbold (1982), Propagating extrusion tectonics in Asia: New insights from simple experiments with plasticine, *Geology*, *10*, 611–616.

Tilmann, F., J. Ni, and INDEPTH-III-SeismicTeam (2003), Seismic imaging of the downwelling Indian lithosphere beneath Central Tibet, *Science*, *300*, 1424–1427, doi:10.1126/science.1082777.

Toussaint, G., E. Burov, and J. Avouac (2004), Tectonic evolution of a continental collision zone: A thermomechanical numerical model, *Tectonics*, *23*(TC6003), 1–24, doi:10.1029/2003TC001604.

Trifonov, V. (1978), Late quaternary tectonic movements of western and central Asia, *Bull. Geol. Soc. Am.*, *89*(7), 1059–1072.

van Hinsbergen, D., P. Kapp, G. Dupont-Nivet, P. C. Lippert, P. G. DeCelles, and T. Torsvik (2011), Restoration of Cenozoic deformation in Asia and the size of Greater India, *Tectonics*, *30* (5), 1–31, doi: 10.1029/2011TC002908.

von Seggern, D. H. (2009), Direct empirical estimation of arrival-time picking error from waveform cross-correlations, *Bull. Seismol. Soc. Am.*, *99*(5), 2749–2758, doi:10.1785/0120080304.

Waldhauser, F., and W. Ellsworth (2000), A double-difference earthquake location algorithm: Method and application to the Northern Hayward fault, California, *Bull. Seismol. Soc. Am.*, *90* (6), 1353–1368, doi: 10.1785/0120000006.

Wessel, P., and F. Smith (1998), New, improved version of generic mapping tools released, *Eos Trans. AGU*, *79* (47), 579–579, doi:10.1029/98EO00426.

Withers, M., R. Aster, C. Young, J. Beiriger, M. Harris, S. Moore, and J. Trujillo (1998), A comparison of select trigger algorithms for automated global seismic phase and event detection, *Bull. Seismol. Soc. Am.*, *88*(1), 95–106.

Wittlinger, G., J. Vergne, P. Tapponnier, V. Farra, G. Poupinet, M. Jiang, H. Su, G. Herquel, and A. Paul (2004), Teleseismic imaging of subducting lithosphere and Moho offsets beneath western Tibet, *Earth Planet. Sci. Lett.*, *221*(1-4), 117–130, doi:10.1016/S0012-821X(03)00723-4.

Wittlinger, G., V. Farra, G. Hetényi, J. Vergne, and J. Nábelek (2009), Seismic velocities in Southern Tibet lower crust: A receiver function approach for eclogite detection, *Geophys. J. Int.*, *177* (3), 1037–1049, doi:10.1111/j.1365-246X.2008.04084.X.

Yin, A., and T. M. Harrison (2000), Geologic evolution of the Himalayan-Tibetan orogen, *Annu. Rev. Earth Planet. Sci.*, *28* (1), 211–280, doi: 10.1146/annurev.earth.28.1.211.

Yuan, X., J. Ni, R. Kind, J. Mechie, and E. Sandvol (1997), Lithospheric and upper mantle structure of southern Tibet from a seismological passive source experiment, *J. Geophys. Res.*, *102*(B12), 27,491–27,500.

Zandt, G., H. Gilbert, T. J. Owens, M. Ducea, J. Saleeby, and C. H. Jones (2004), Active foundering of a continental arc root beneath the southern Sierra Nevada in California, *Nature*, *431*, 41–46, doi: 10.1038/nature02847.

Zhao, W., et al. (2011), Tibetan plate overriding the Asian plate in central and northern Tibet, *Nat. Geosci.*, *4*(12), 1–4, doi:10.1038/ngeo1309.

Zubovich, A., et al. (2010), GPS velocity field for the Tien Shan and surrounding regions, *Tectonics*, *29*(6), 1–23, doi:10.1029/2010TC002772.